Report No 1942/PH

Analysis of tests of the CASTOR calorimeter prototype

Ewa Gładysz-Dziaduś

1 INTRODUCTION

The CASTOR (Centauro And Strange Object Research) detector has been initially proposed to study the very forward rapidity region in Pb+Pb collisions at the LHC and thus to complement the CERN heavy ion physics program developed essentially in the baryon-free midrapidity region. The CASTOR in the CMS will contribute not only to the heavy ion program [1], but also to diffractive and low-x physics in pp collisions [2]. The CMS and TOTEM experiments supplemented by the CASTOR detector will constitute the largest acceptance system ever built at a hadron collider, having the possibility to measure the forward energy flow [3].

The preliminary schematic design, the description of the detector performance can be found in [4] and its integration in the CMS experiment has been presented in [5].

The comprehensive review [6] by E. Gładysz-Dziaduś summarizes the physical motivation, experimental results which inspired the project and simulations showing its sensitivity to Centauros, strangelets and other exotic phenomena. Simulations of Centauro events have been done by means of our Centauro generator CNGEN, which has been described in [7]. The proposed "exotic" physics of the CASTOR calorimeter and the T2 telescope (being a part of the TOTEM experiment) has been presented by E. Gładysz-Dziaduś at the CMS-Heavy Ion Meeting International Workshop on Physics and Techniques for the LHC and RHIC Experiments, Delphi 2003 [8].

The CASTOR calorimeter prototypes have been constructed and tested with electron beams at CERN/SPS in 2001, 2002 and in June 2003. The purpose of the last test was to investigate the viability of different options, rather that to get the precise and quantitative results. The general view of the CASTOR calorimeter and the photo of the electromagnetic (EM) prototype are shown in Fig. 1. We have tested four readout units of the calorimeter, arranged side-by-side in four azimuthal sectors, each consisting of 10 sampling units. Each sampling unit contained a tungsten plate 5 mm thick and three planes of quartz fibres 640 μm thick [1], in *J1, J2* and *S2* sectors, or alternatively one 1.8 mm thick quartz plate in the sector *S1*. It gives the filling ratios 37.6 % and 30 % for Q-plate and Q-fibres options. The calorimeter has 45^0 orientation relative to the impinging particles, so the total length of the sector with quartz plates was $\sim 0.83\ \lambda_{int} \sim 23.7\ X_0$. Different options and technical solutions have been investigated, as shown in Fig. 2.

In particular, we have checked the light transmittance in light guides with two different reflectors: HF-reflecting foil (Dupond + SiO_2 + TiO_2) and a glass reflector (Al + MgFr). We investigated the response of the calorimeter, by using different types of light-reading devices, i.e. two different kinds of avalanche photodiodes (APDs): Hamamatsu S8148 (APD1) and Advanced Photonic DUV (APD2) and two different photomultipliers (PMTs): Hamamatsu R374 and Philips XP2978. With electrons of energies between 20 and 200 GeV, we have studied a linearity of calorimeter response with energy and relative energy resolution for quartz fibres (Q-F) and quartz plates (Q-P). The calorimeter was placed on a platform movable with respect to the electron beam in both horizontal and vertical directions. A telescope of two wire chambers in front of the calorimeter was used to measure the electron impact point.

The preliminary results of the analysis have been already presented at the CMS meetings [5]. Here a more precise analysis, based on the procedure used in the previous CASTOR prototype tests and taking into account a beam profile has been applied. We

[1] 600 μm of a quartz core and 40 μm of a silicon cladding

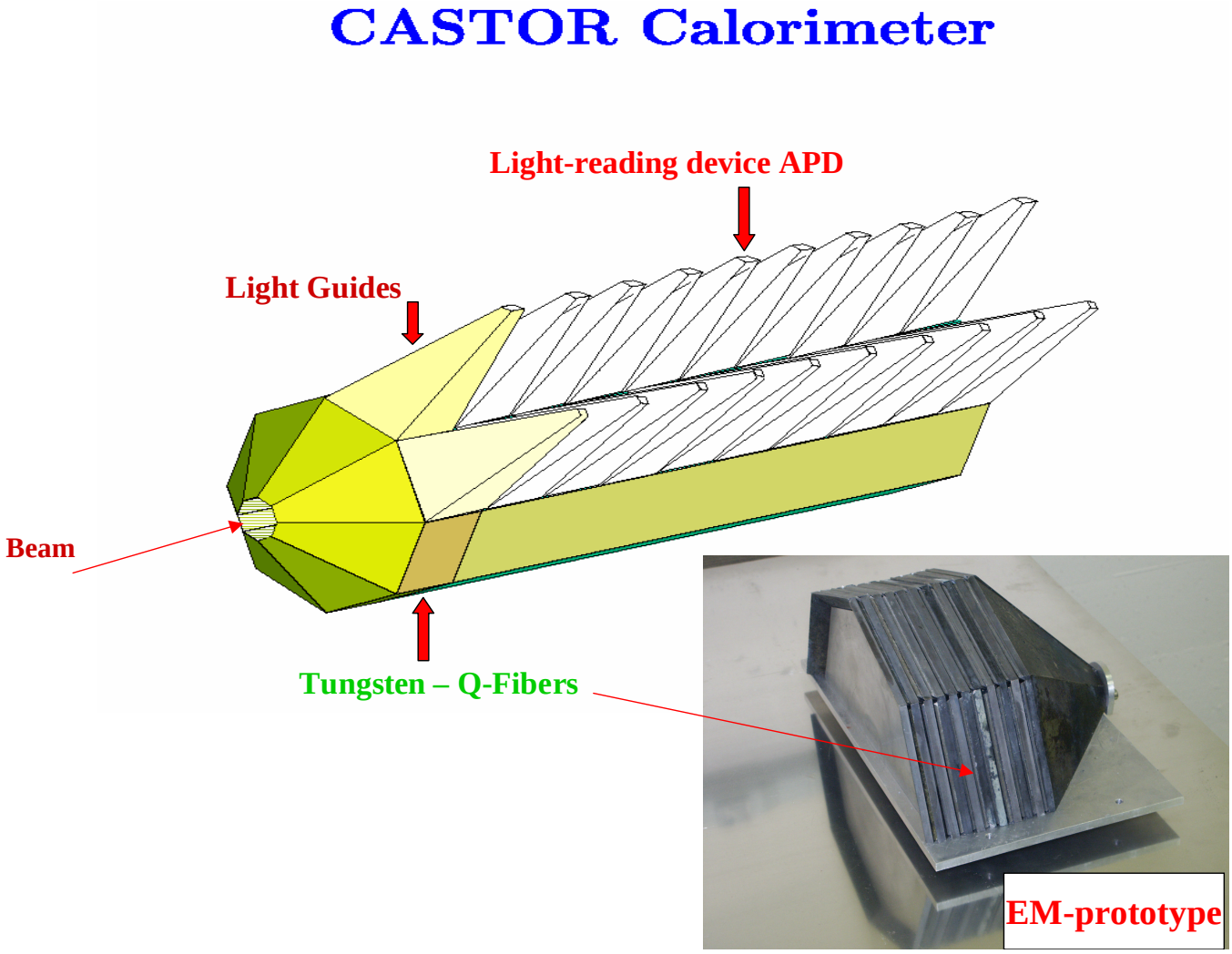

Figure 1: The CASTOR calorimeter scheme and photo of the EM prototype [5].

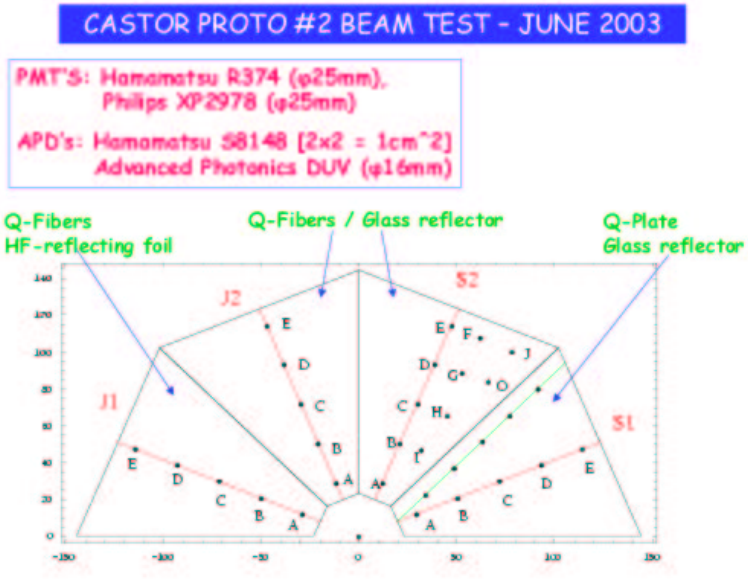

Figure 2: Different options investigated in the beam test in 2003 [5].

found a good linearity of response with energy for the calorimeter with quartz fibres as well as with quartz plates and a good reflectance of a HF-reflecting foil. Advanced Photonic APDs seem to be a very realistic option for the light-reading device. Following the results of the tests the modified version of the CASTOR calorimeter, with APDs instead of PMTs and HF-reflecting foil instead of the glass mirror is being considered [5].

2 Linearity and energy resolution

To study linearity of a calorimeter response with energy and a relative energy resolution, the central points C (Fig. 2) in different azimuthal sectors have been exposed to electron beams of energy 20, 40, 80, 100, 150 and 200 GeV. The results of energy scanning, analysed for four calorimeter options, are shown in the following figures:

1. *Sector S1* - Quartz Plate, glass reflector, Philips PMT, central point C:
   Figs. 3, 4, 5.

2. *Sector S2* - Quartz Fibres, glass reflector, Philips PMT, central point C:
   Figs. 6, 7, 8.

3. *Sector J2* - Quartz Fibres, glass reflector, Hamamatsu APD, central point C:
   Figs. 9, 10, 11.

4. *Sector S1* - Quartz Plate, glass reflector, Advanced Photonic APD, central point C:
   Figs. 12, 13, 14.

Distributions of signal amplitudes, after introducing the cuts accounting a profile of the beam, are in most cases symmetric and well fitted by a gaussian function (Figs. 3, 6, 9, 12). Asymmetry of few distributions was partly caused by the wide spread of the beam in these events.

The calorimeter response turns out to be linear in the explored energy range. The average signal amplitude ADC , expressed in units of ADC channels, has been satisfactorily fitted by the following formula:

$$ADC = a + b * E \tag{1}$$

where energy E is expressed in GeV.

The fitted values of the parameters are shown in the Table 1.

Relative energy resolution of the calorimeter has been studied by analysis of σ/E vs. E (GeV) plots, which have been fitted by two different expressions [9, 10]:

$$\sigma/E = p_0 + p_1/\sqrt{E} \tag{2}$$

$$\sigma/E = p_0 \oplus p_1/\sqrt{E} \oplus p_2/E \tag{3}$$

where the mark $\oplus$ means that the terms have been added in quadrature.

Three terms determine the characteristic of the energy resolution. The constant term p_0, coming from the gain variation with changing voltage and temperature, limits the resolution at high energies. To the stochastic term p_1 due to intrinsic shower fluctuations, photon statistics contributes. The p_2 term contains the noise contribution from capacitance and dark current.

Generally, both formulae satisfactorily fit the data (see Table 1). The important point is that the constant term p_0 is close to 0 for all options. Also the stochastic term p_1, being less than 38 % for the *S1* sector seems to be reasonable, when compared to $p_1 = (36.2 \pm 0.2)$ %, obtained in [11] for the calorimeter prototype of similar geometry and technology. The readout by photodiodes leads to p_2 term, measured to be 1.25 GeV and 4.5 GeV for Advanced Photonic APD and Hamamatsu APD respectively. It should be noted that the APDs are very sensitive to both voltage and temperature changes but in this test there was no their stabilization.

3 Area scanning

The purpose of area scanning was to check the uniformity of the calorimeter response, generated by electrons hitting points located at different places of the sector area, the possible "edge" effects, a lateral leakage from the calorimeter and a cross-talk between neighbouring sectors.

3.1 Area scanning of the sector S2

For the area scanning of the sector *S2* (Q-Fibres, glass), connected to a Philips PMT, central points (A-E) as well as border points (I-O) (see Fig. 2) have been exposed to electron beam of energy 100 GeV. Distributions of signal amplitudes are shown in Figs. 15 and 16 for central and border points respectively. The distributions are symmetric

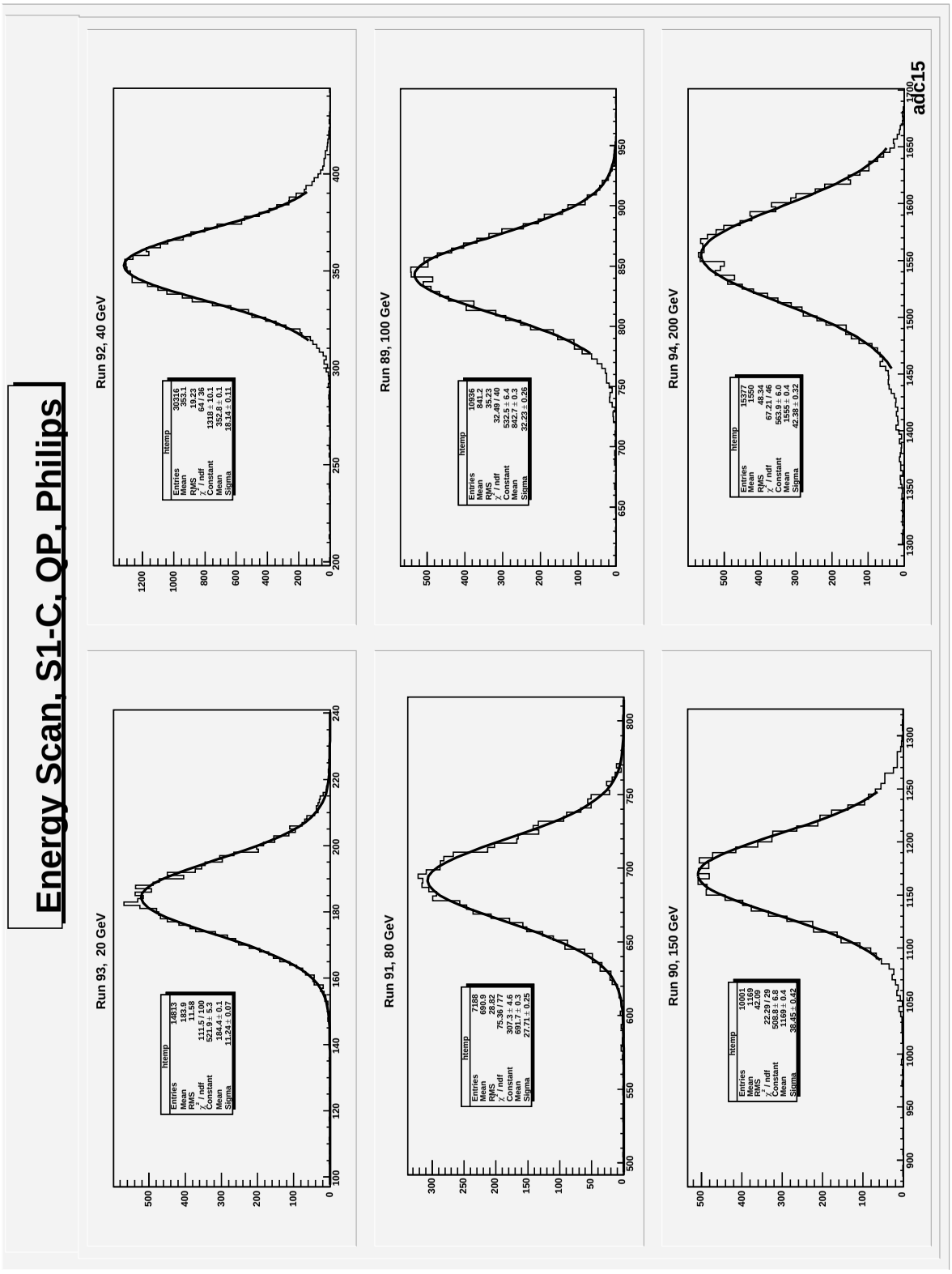

Figure 3: Distributions of signal amplitudes, expressed in ADC channels. The central point C of the sector *S1* (Quartz Plate, glass, Philips PMT) has been exposed to electron beams of several energies.

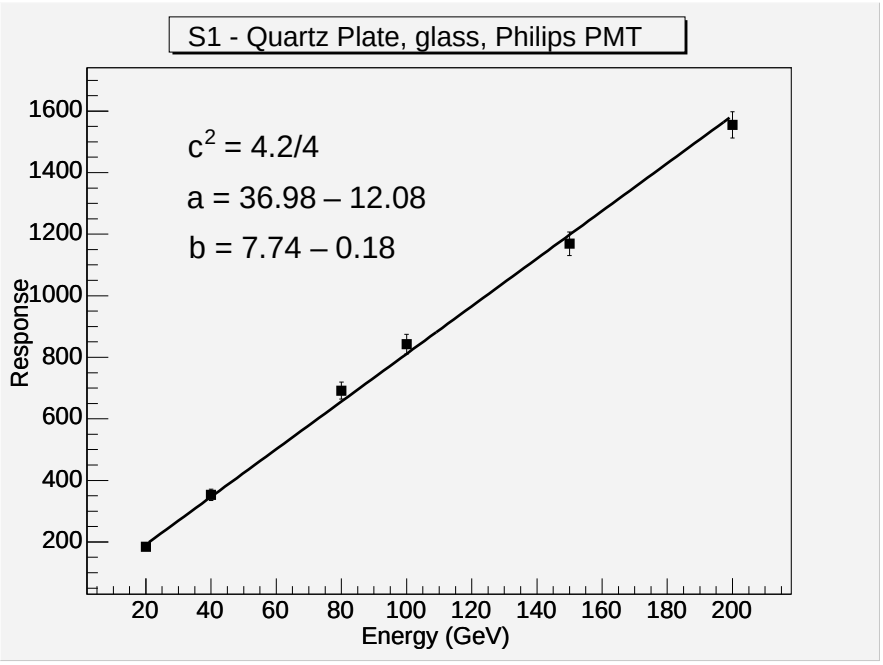

Figure 4: Linearity in the sector *S1*: Quartz Plate, Philips PMT, central point C.

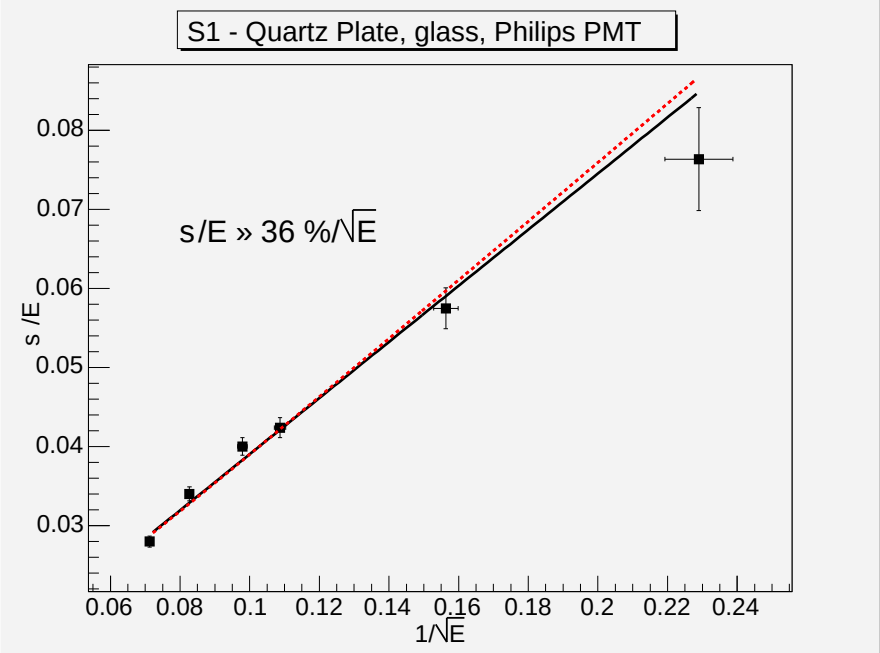

Figure 5: Energy resolution in the sector *S1*: Quartz Plate, Philips PMT, central point C. Two fits are shown: $\sigma/E = p_0 + p_1/\sqrt{E}$ -black line ; $\sigma/E = p_0 \oplus p_1/\sqrt{E} \oplus p_2/\sqrt{E}$ - red dashed line.

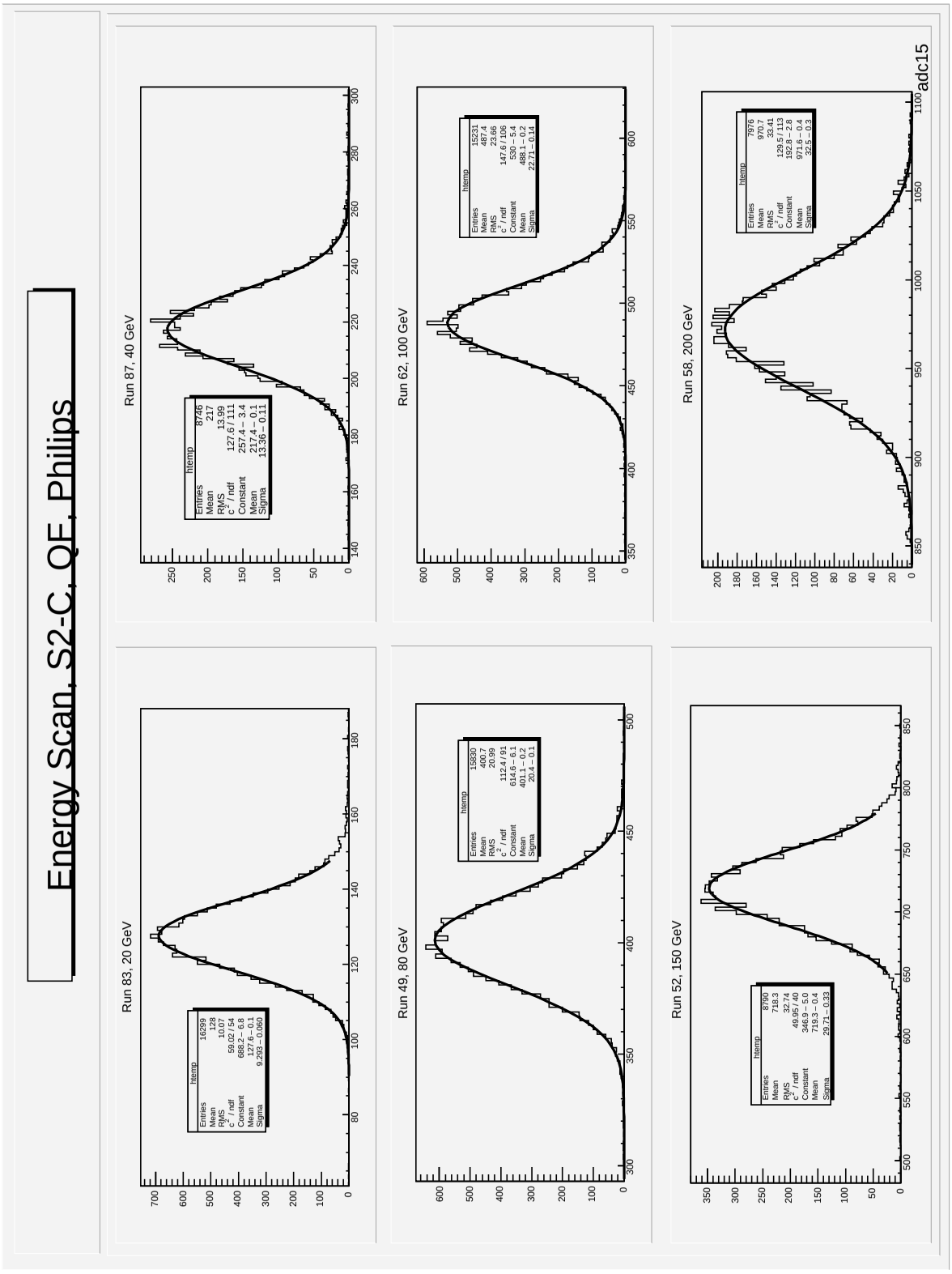

Figure 6: Distributions of signal amplitudes, expressed in ADC channels. The central point C of the sector *S2* (Quartz Fibres, glass, Philips PMT) has been exposed to electron beams of several energies.

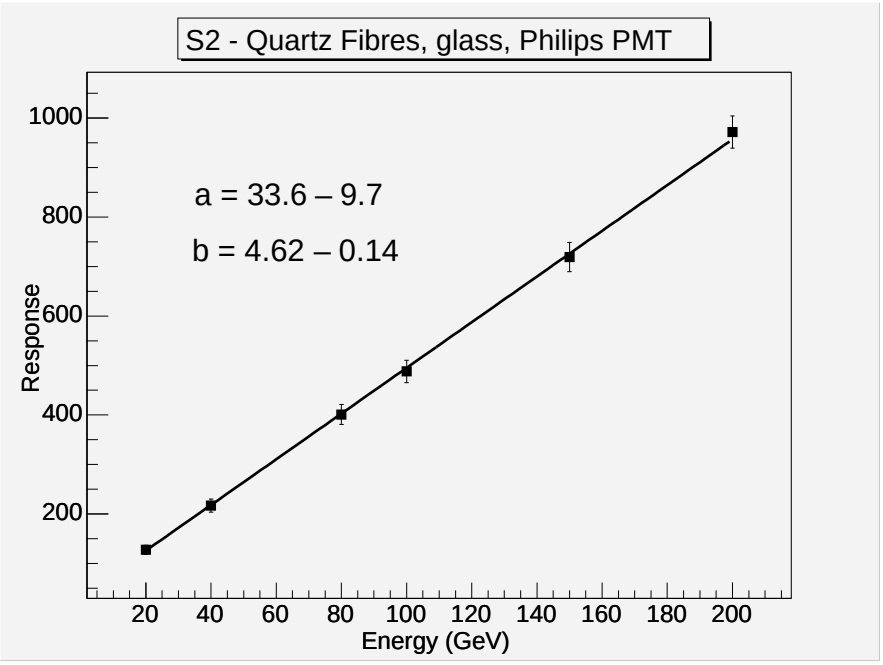

Figure 7: Linearity in the sector S2: Quartz Fibres, Philips PMT, central point C.

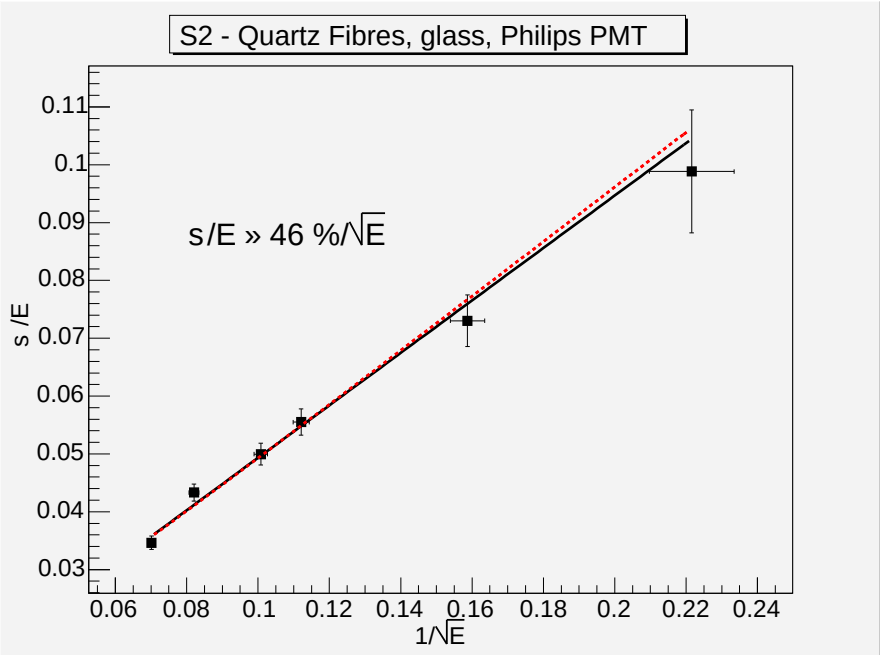

Figure 8: Energy resolution in the sector S2: Quartz Fibres, Philips PMT, central point C. Two fits are shown: $\sigma/E = p_0 + p_1/\sqrt{E}$ -black line ; $\sigma/E = p_0 \oplus p_1/\sqrt{E} \oplus p_2/\sqrt{E}$ - red dashed line.

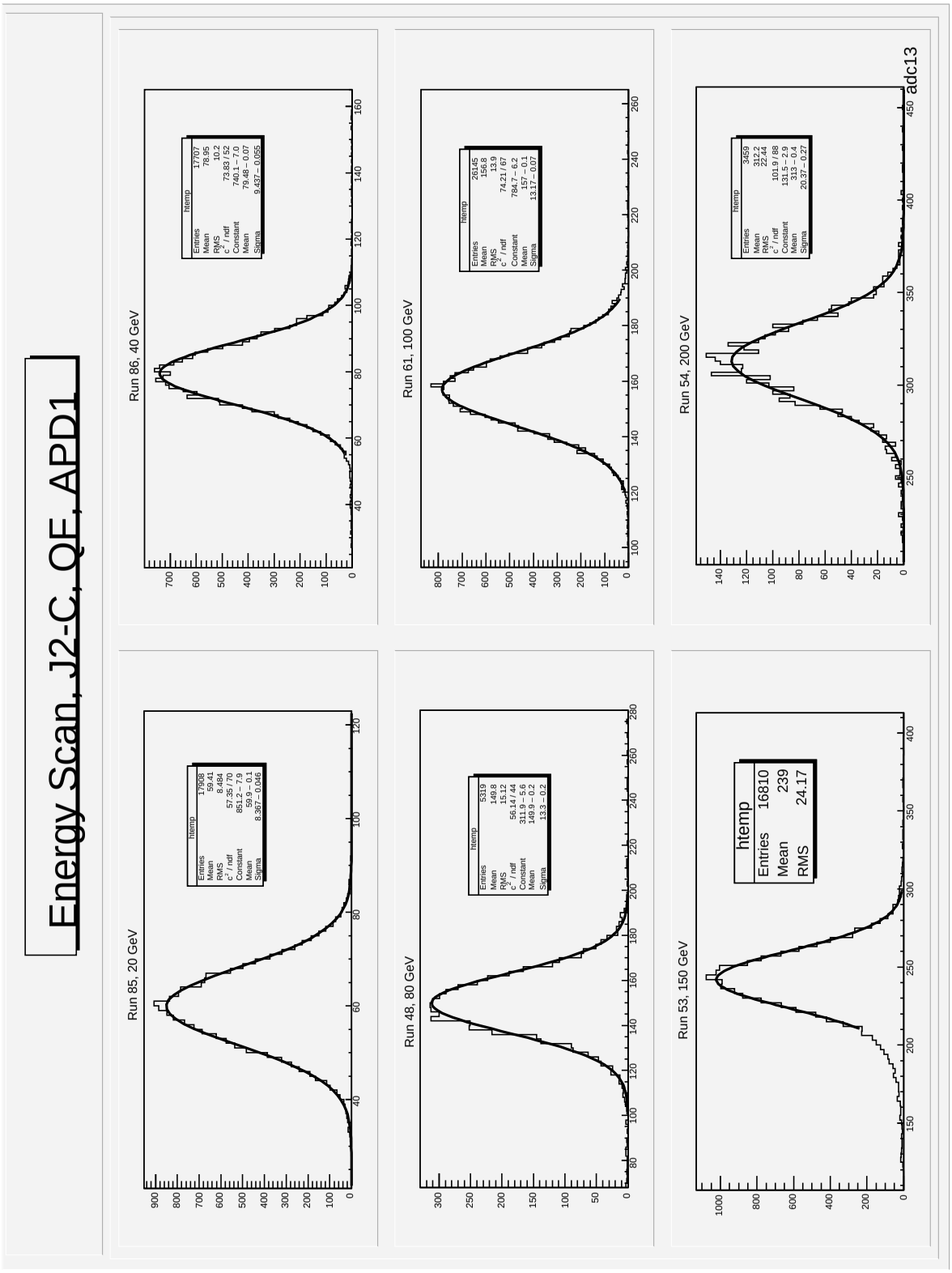

Figure 9: Distributions of signal amplitudes, expressed in ADC channels. The central point C of the sector *J2* (Quartz Fibres, glass, Hamamatsu APD) has been exposed to electron beams of several energies.

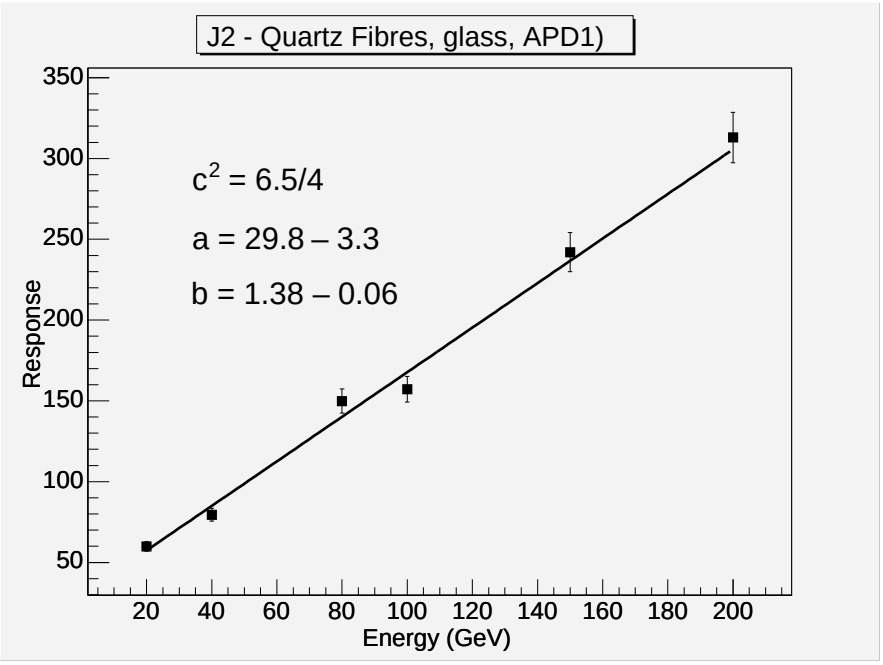

Figure 10: Linearity in the sector J2: Quartz Fibres, Hamamatsu APD, central point C.

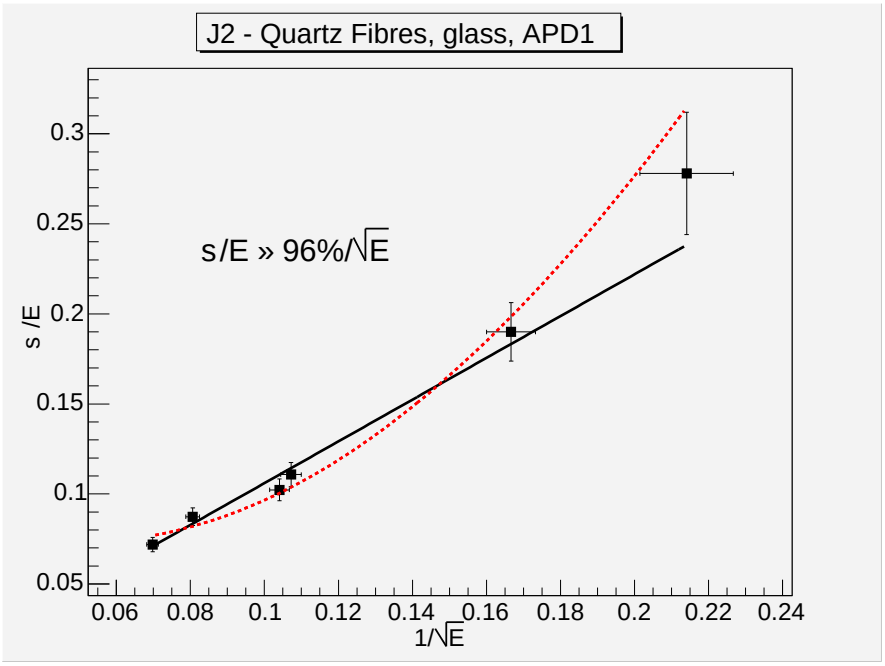

Figure 11: Energy resolution in the sector J2: Quartz Fibres, Hamamatsu APD, central point C. Two fits are shown: $\sigma/E = p_0 + p_1/\sqrt{E}$ -black line ; $\sigma/E = p_0 \oplus p_1/\sqrt{E} \oplus p_2/\sqrt{E}$ - red dashed line.

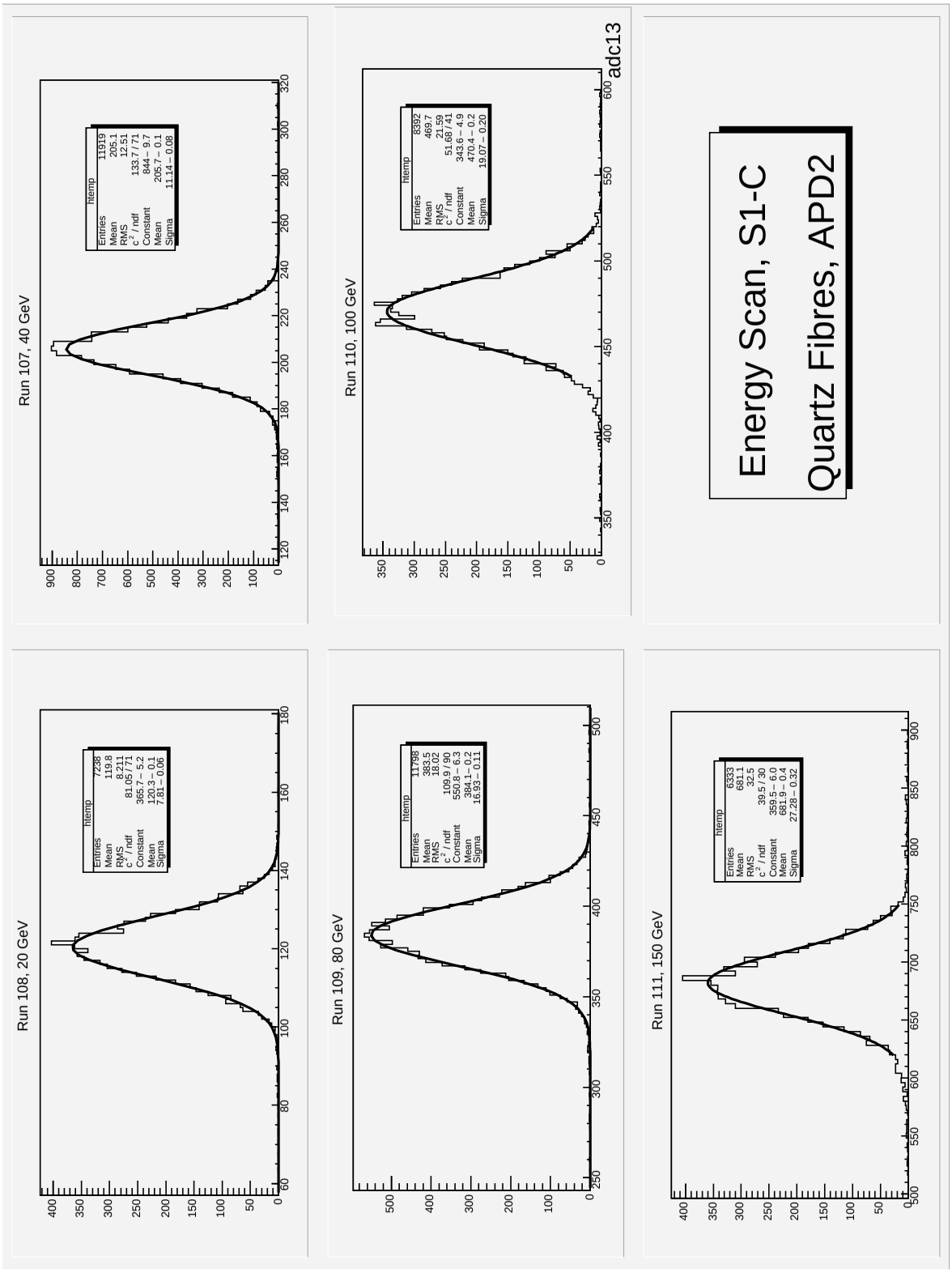

Figure 12: Distributions of signal amplitudes, expressed in ADC channels. The central point C of the sector *S1* (Quartz Plate, glass, Advanced Photonic APD) has been exposed to electron beams of several energies.

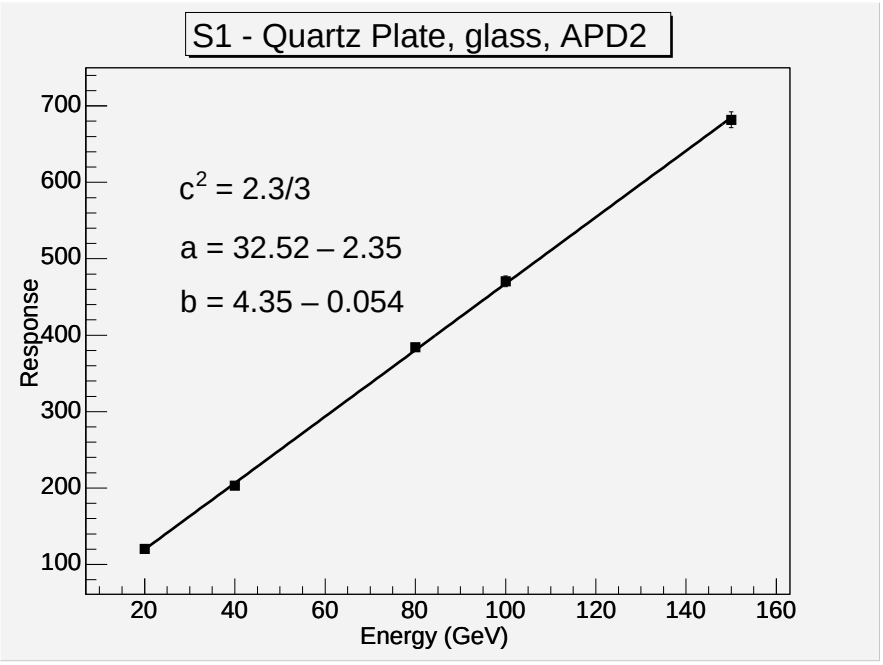

Figure 13: Linearity in the sector *S1*: Quartz Plate, APD2, central point C.

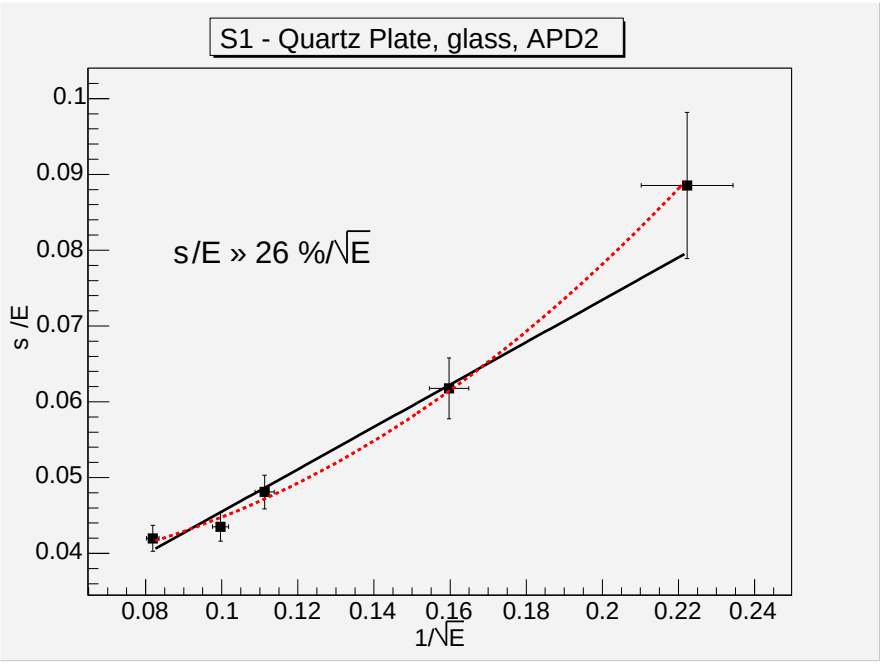

Figure 14: Energy resolution in the sector *S1*: Quartz Plate, Advanced Photonic APD, central point C. Two fits are shown: $\sigma/E = p_0 + p_1/\sqrt{E}$ -black line ; $\sigma/E = p_0 \oplus p_1/\sqrt{E} \oplus p_2/\sqrt{E}$ - red dashed line.

and well described by Gaussian fits for majority of investigated points. Asymmetric distributions are seen only for points closer than ~ 3 mm from the calorimeter outer edge or the sector border.

Fig. 17 shows dependence of the average calorimeter response and relative resolution (σ/E) on the distance R from the calorimeter center, for both central and border points. The upper picture shows coordinates of the points, corrected for the beam impact point position. It is seen that points E, F, J practically lie at the edge of the calorimetr. The raise of signal amplitudes as well as of distribution widths with R can be caused by a lateral spread of a beam. For large R a substantial part of beam electrons is outside of the calorimeter sector and can fall directly to the light guides. The picture at the right lower pad shows that the relative energy resolution practically does not depend on the position of the impact points (with exception of the points E, F, J, located very close to the calorimeter edge) and it is at the level of ~ 4.6 % for 100 GeV electrons.

3.2 S1 - S2 cross talk

10 points (runs 113 - 122), located at distances $\simeq$ 2.5-32 mm from the *S1* (QP, glass)/*S2* (QF, glass) sector border, have been exposed to electron beam of energy 80 GeV. The simultaneous readout of both sectors have been done by Advanced Photonic APD and Hamamatsu PMT in *S1* and *S2* respectively. The upper left pad of Fig. 18 shows the coordinates of the measured points, in the calorimeter frame, when corrected for the beam impact point position. The star marks the coordinates of the border point, between *S1* and *S2* sectors, found from dependence of signal amplitudes on X(Y) coordinates (lower pads).

Fig. 19 shows that distributions of signal amplitudes in the *S2* sector, for points distanced from the sector border more than ~ 8 mm, are symmertic (Gaussian) and a leakage to the *S1* sector is negligible. The relative energy resolution σ/E is of the order ~ 2.9 % for 80 GeV electrons.

The observed leakage between *S1* and *S2* sectors is shown in Figs. 20 and 21. Dependences of the calorimeter response, leakage fraction and relative energy resolution σ/response on the distance d from the sector border, for *S1* (runs 118-121) and *S2* sectors (runs 113 - 117, 122) are shown in Fig. 22. Close to the sector border, both a light output and energy resolution are a little better for *S2*-Quartz Fibres sector connected to Hamamatsu PMT ($\sigma/E \simeq 2.9$ %) than for *S1*-Quartz Plate sector connected to Advanced Photonic APD ($\sigma/E \simeq 4.5$ %). At distances exceeding ~ 14 mm a lateral leakage to the neighbouring sectors is practically negligible.

3.3 Comparison of J1, J2 and S1 sectors

For comparison of the uniformity of calorimeter response, several points located at different places of the sectors area have been exposed to electron beam of energy 80 GeV. The points A-E at the middle of *J1, J2* and *S1* sectors and points 4-8 at the border part of the *S1* sector (see Fig. 2) have been studied. All sectors have been connected to Hamamatsu PMT. Distributions of signals are shown in the following figures:

1. *J1* - Quartz Fibres, foil, Hamamatsu PMT, Fig. 23;

2. *J2* - Quartz Fibres, glass, Hamamatsu PMT, Fig. 24;

3. *S1* - Quartz Plate, glass, Hamamatsu PMT, sector centre, Fig. 25;

4. *S1* - Quartz Plate, glass, Hamamatsu PMT, sector border, Fig. 26.

Symmetric and Gaussian distributions of signal amplitudes in the middle of the sectors and asymmetric distributions close to the sector border (points 4-8) and sometimes (*J1* sector) also close to the inner (point A) and outer (point E) calorimeter edge are observed. The beam profile correction reduces asymmetry. Also some leakage from the *S1* to the neighbouring sector, for border points (4-8), is seen.

Comparison of a light output and a relative energy resolution for all studied options is shown in Figs. 27 and 28 respectively. Light output is the highest in the *S1* (QP - glass) sector, and it is practically the same for the central and for the border points. It depends weakly on the position of the impact point: for the *S1* a weak decrease, and for the *J1* and *J2* sectors a weak increase of the calorimeter response with a distance R from the calorimeter center is observed.

The relative energy resolution is almost independent of the position of the impact point and it is $\sim$ 1.5-2.5 % for *S1* (QP-glass) and *J2* (QF-glass) sectors and $\sim$ 3.5-4.0 % for J2 (QF-foil) to 80 GeV electrons.

4 SUMMARY

1. Comparison the quartz plate with quartz fibres suggests that a calorimeter with a quartz plate is a promising option, although it needs some further investigation.

   - Good linearity of response with energy is observed for both options.
   - Q-plate gives more the light output than equal thickness Q-fibres (Fig. 27).
   - Relative energy resolution is not worse for the solution with quartz plates. At *S1*-QP as well as *J2*-QF sectors, both connected to Hamamatsu PMT, we found the similar energy resolution, $\sim$ 2 %, to 80 GeV electrons (Fig. 28). Comparing quartz plates to quartz fibres both connected to the Philips PMT and with using the same glass reflector in the light guides (Figs. 5 and 8, Table 1), we see that the constant term p_0, that limits performance at high energies, is less than 1% in both options. The stochastic term $p_1 \simeq 36$ % and 45 % for quartz plates and quartz fibres respectively. It means that we would measure an electromagnetic energy hitting the CASTOR in Pb+Pb collisions at the LHC ($\sim$ 40 TeV according to the HIJING predictions) well below 0.5 %. Also the exotic objects, whose energy is expected to be higher than several TeV [4, 6] could be measured with sufficient precision. These values of the parameter p_1 are comparable to $p_1 = (36.2 \pm 0.2)$ %, obtained for the calorimeter prototype of similar geometry and technology [11]. On the other hand, comparison between the CASTOR prototype and the NA52, H1 and other electromagnetic calorimeters which employ similar quartz fibres technology, but the geometries are different [9, 10], shows that there is room for improvement of the stochastic term, what can be profitable in realization of p + p physics.

- Some leakage from the *S1* (Q-plate) sector to the neighbouring *S2* (Q-fiber) sector, for impact points closer than 20 mm from the sector border, is observed (Figs. 18, 20, 21, 22).

2. The APDs appear to be a realistic option for the light-reading device, although they still need more investigation (radiation-hardness and cooling tests).

3. The relative energy resolution is weakly dependent on the position of the impact point at the sectors containing quartz fibres as well as quartz plates (Fig. 28).

4. The light output is a little higher for the glass reflector, than that for the HF-foil, with using the Hamamatsu PMT as the light reading device (Fig. 27). However, the HF-reflecting foil has better reflectance in the region of high quantum efficiency of APD (λ >400 nm) than glass mirror [5], so the option using simultaneously both a HF-foil and APDs seems to be worth consideration.

These results inspired some modifications in the CASTOR calorimeter design. The considered modified design, based on the Q-plates, APDs and HF-reflecting foil has been presented at CMS meetings [5].

Acknowledgments

I would like to thank my colleagues X. Aslanoglou, A. Cyz, N. Davis, Y. Musienko, and A. Panagiotou with whom we have tested together the CASTOR calorimeter prototype, and also acknowledge the staff of the STREAM calorimeter, especially Heejong Kim, for their help during the tests and decoding the data. Thanks Marina Golubieva for her advices concerning the analysis of the data and J. Bartke for reading the manuscript and editor corrections. This work was partly supported by Polish State Committee for Scientific Research grant No. 2P03B 057 24 and SPUB-M/CERN/P03/DZ1/2000-2002.

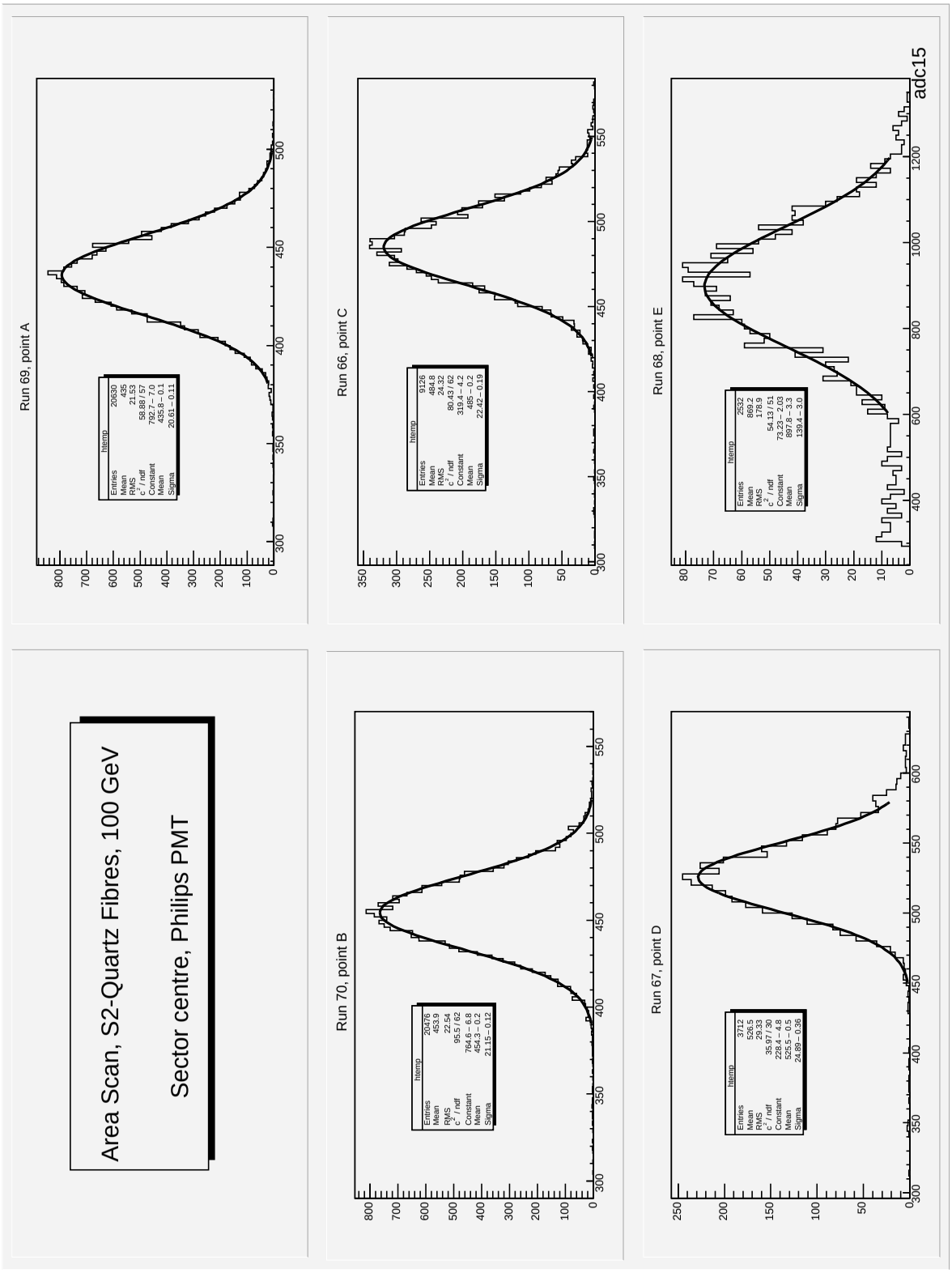

Figure 15: Calorimeter response to 100 GeV electrons in the centre of the sector *S2*: Quartz Fibres, Philips PMT, points A-E.

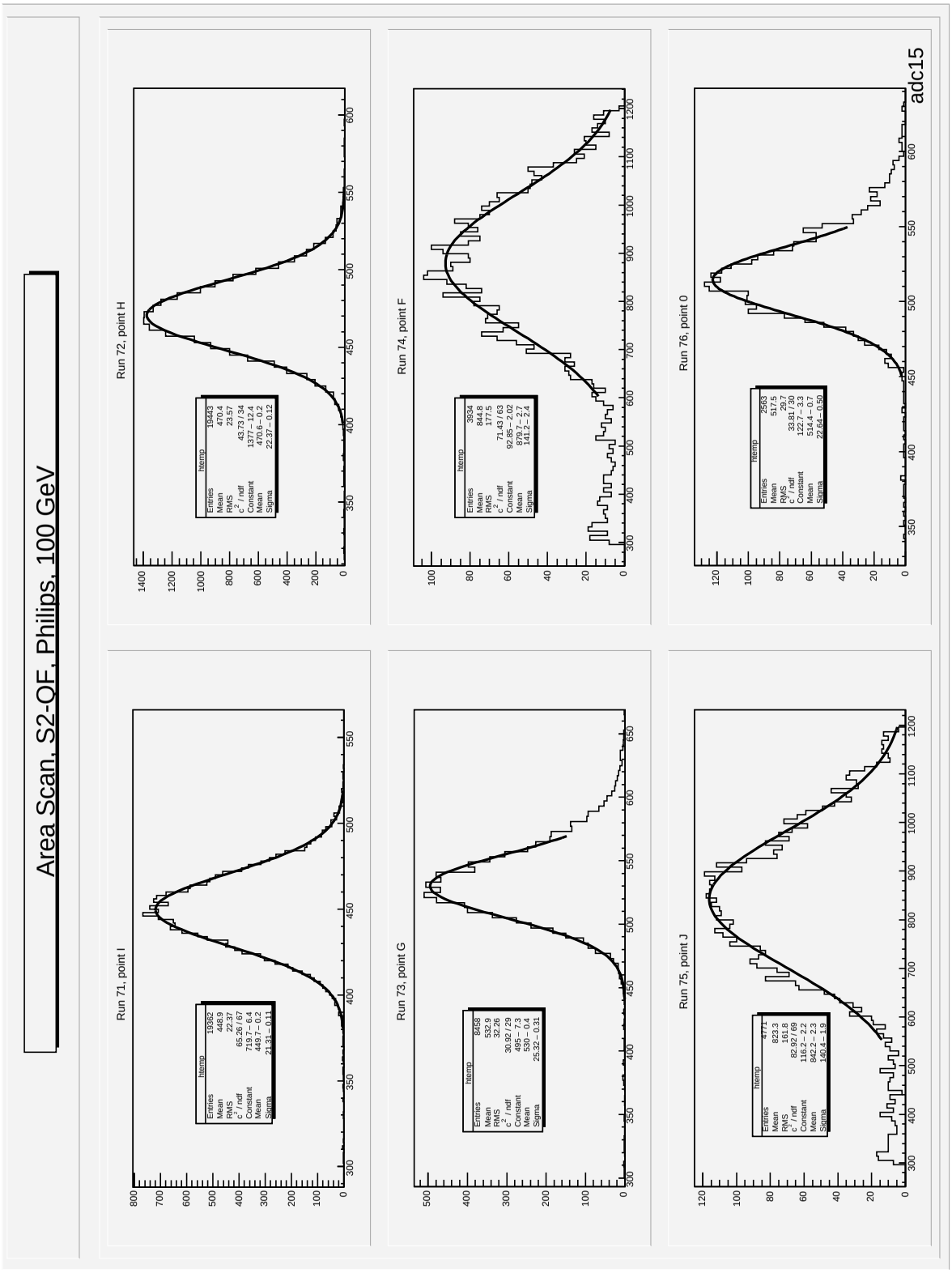

Figure 16: Calorimeter response to 100 GeV electrons in the sector *S2*: Quartz Fibres, Philips PMT. Points (F-J and O) are close to the border of *S2* and *S1* sectors.

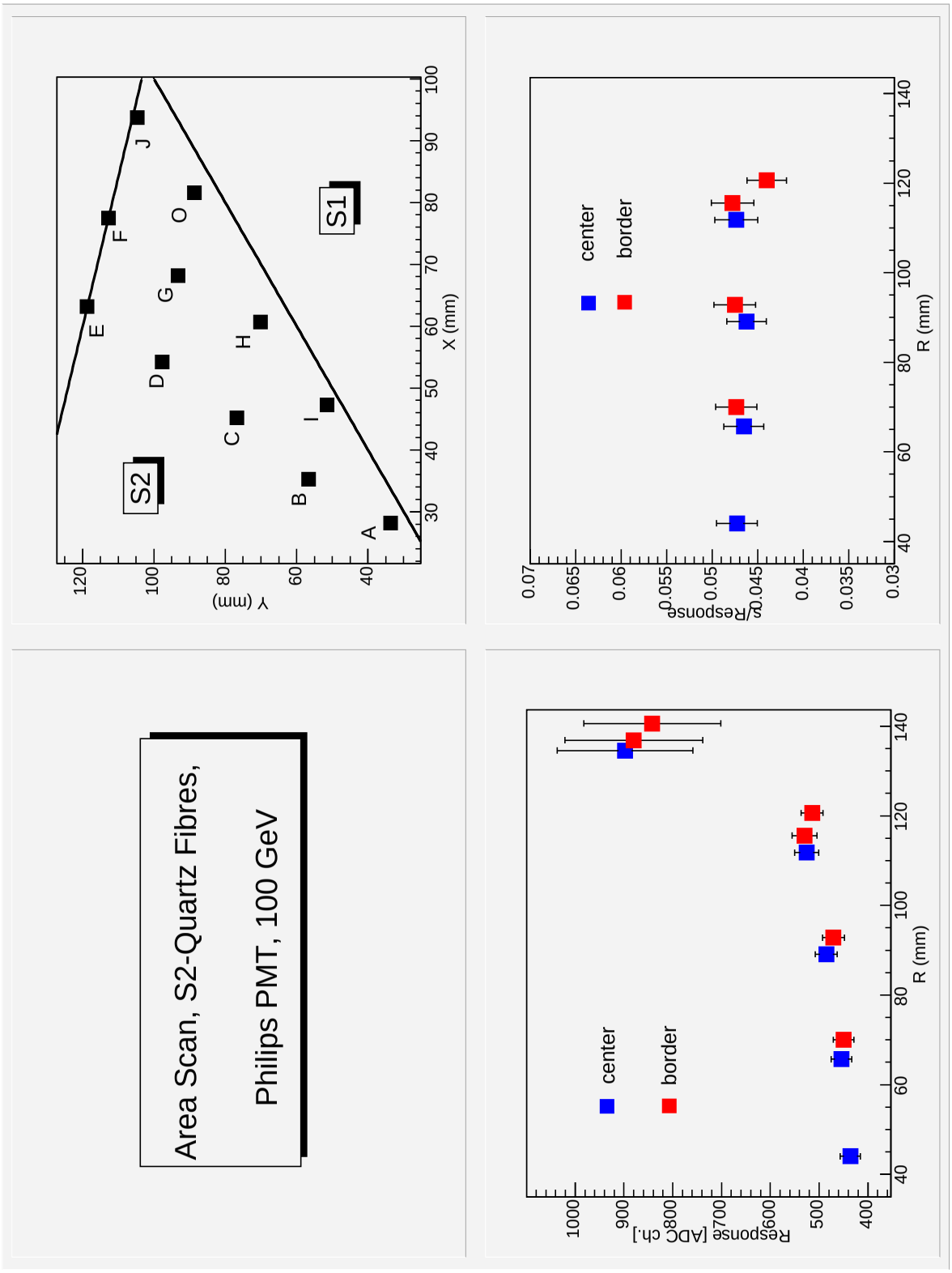

Figure 17: Dependence of the average signal amplitude on the distance R from the calorimeter center in the sector *S2*: Quartz Fibres, Philips PMT. Response to 100 GeV electron beam, hitting the central (A-E) and the border (I-O) points, are shown.

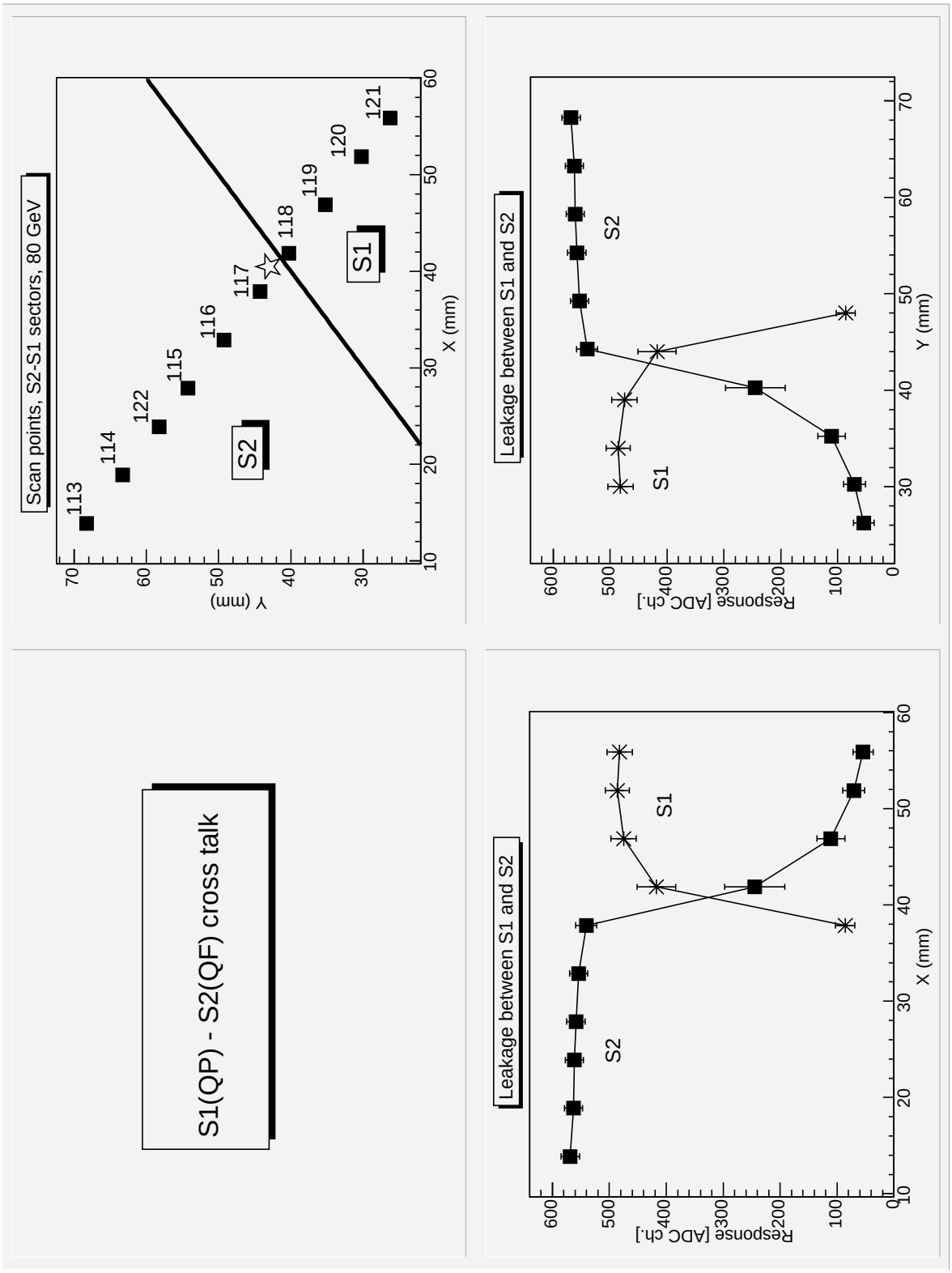

Figure 18: Calorimeter response vs. X (Y) coordinates, in the sectors: *S1* (QP, APD2) and *S2* (QF, Hamamatsu PMT) for several points at distances $\simeq$ 2.5-32.0 mm from the sector border. The upper left pad shows the position of the points in the calorimeter frame, corrected for the beam impact points. The star marks the coordinates of the sectors border point, found from dependence of signal amplitudes on X(Y) coordinates (lower plots).

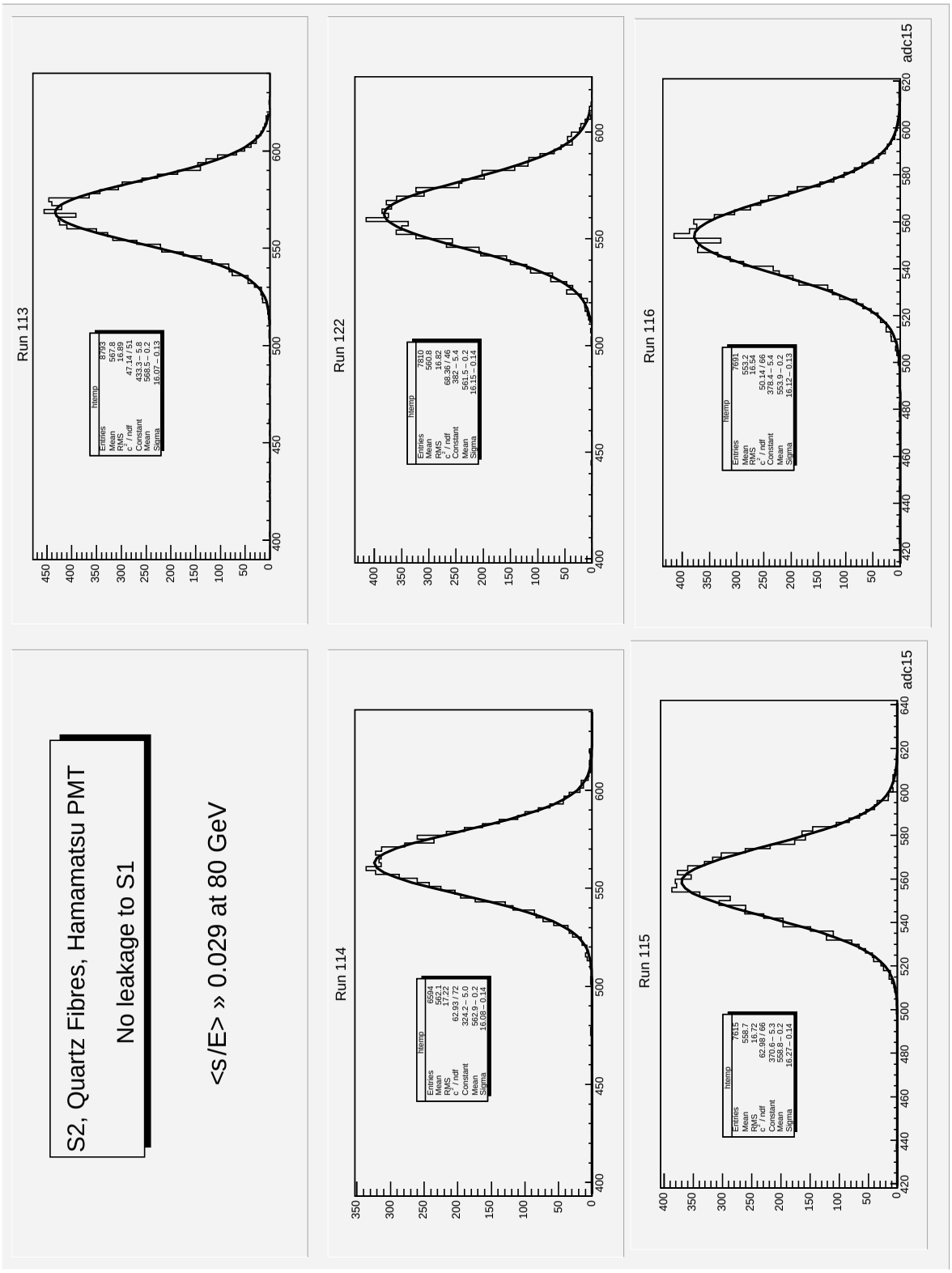

Figure 19: Calorimeter response in the sector *S2* (Quartz Fibres, Hamamatsu PMT) for 5 points at distances $\simeq$ 8 -32 mm from the border.

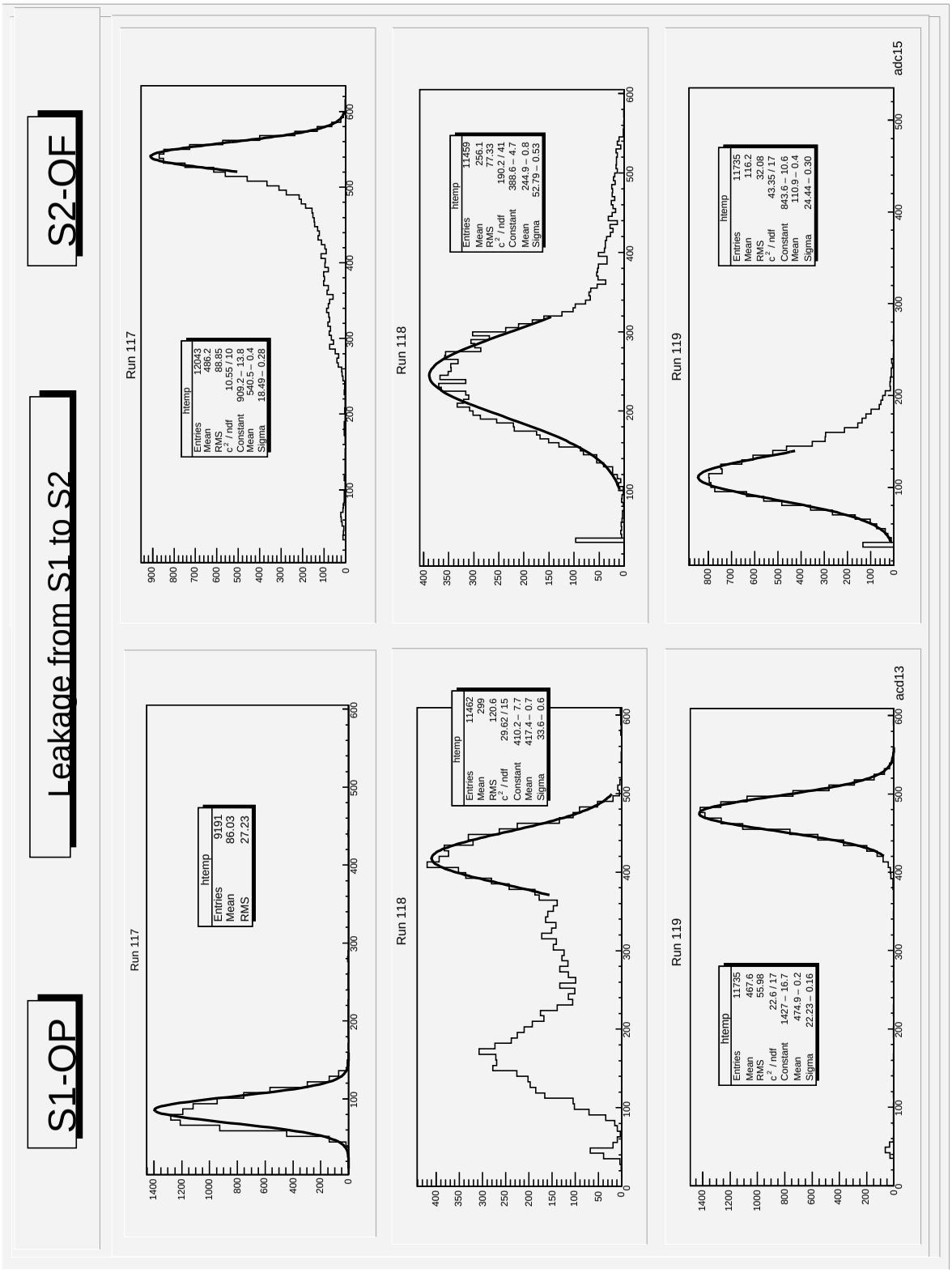

Figure 20: Calorimeter response in the sectors: *S1* (QP, APD2) and *S2* (QF, Hamamatsu PMT) for three points at distances $\simeq$ 2.5 - 8 mm from the border.

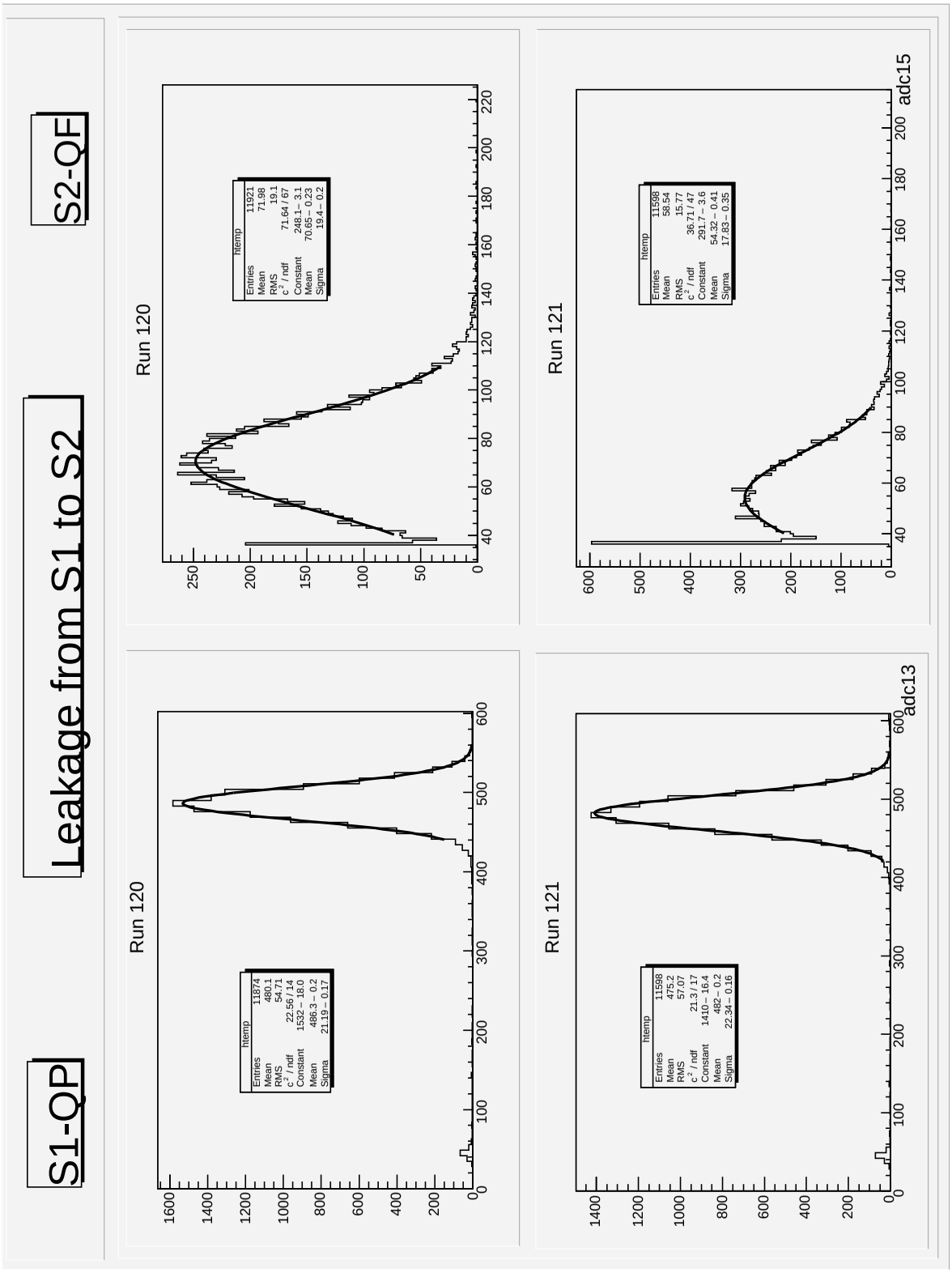

Figure 21: Leakage from the *S1*(QP, APD2) to *S2*(QF, Hamamatsu PMT) for two points distanced far than 14 mm from the sector border.

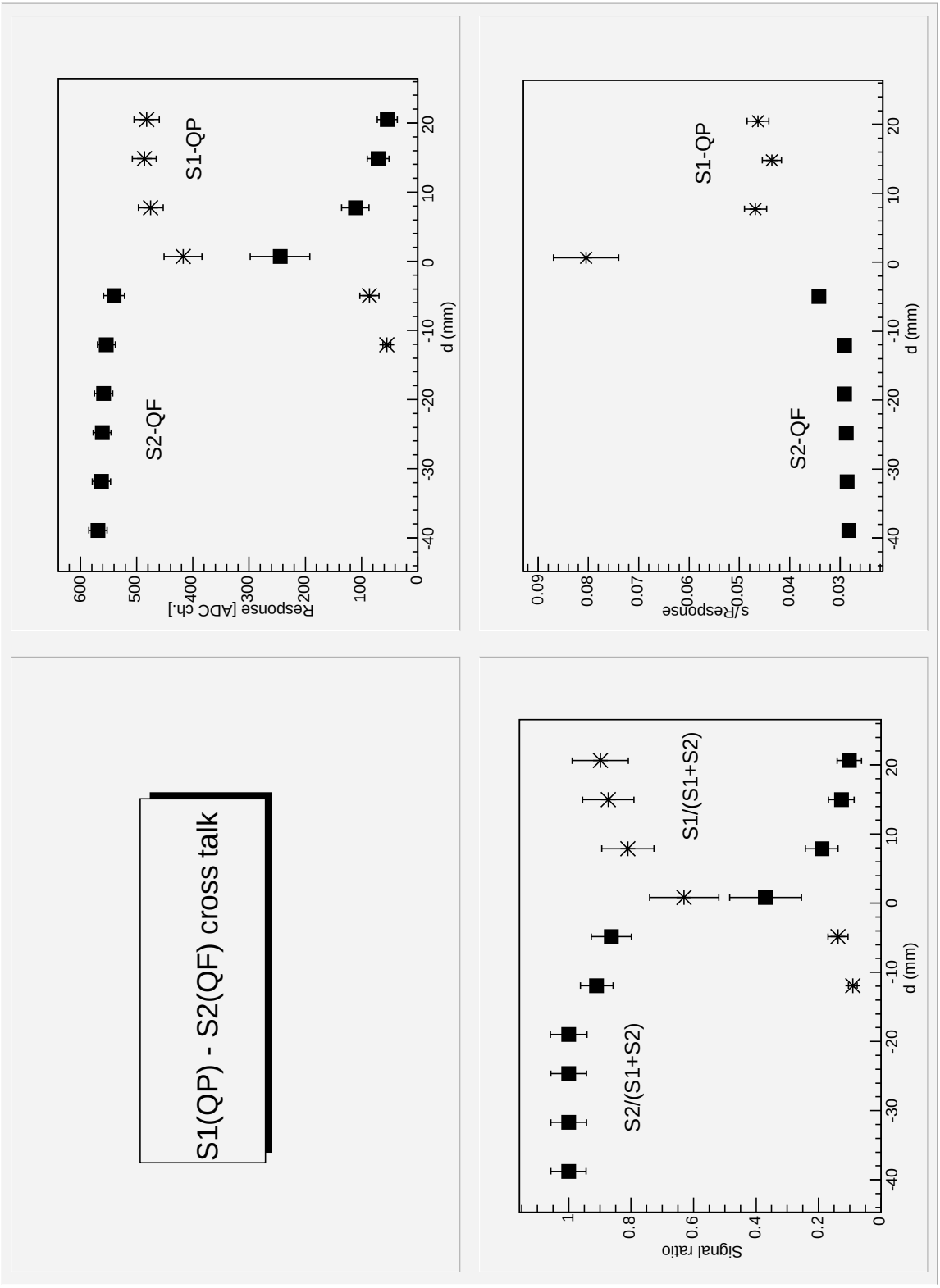

Figure 22: Comparison of the calorimeter response and the resolution (σ/response) in the sectors: *S1* (QP, APD2) (runs 118-121) and *S2* (QF, Hamamatsu PMT) (runs 113-117, 122) for points at different distances d from the sector border.

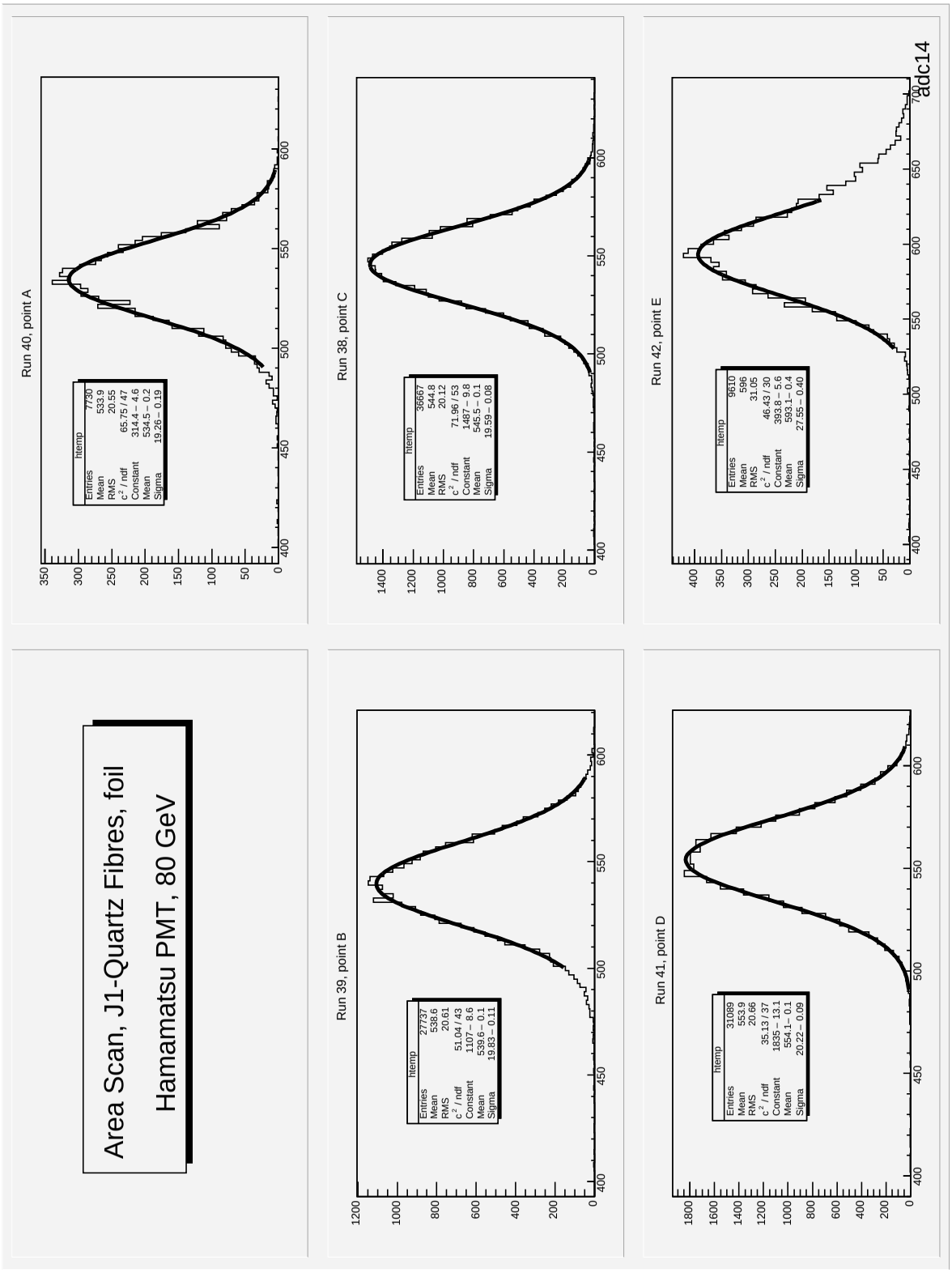

Figure 23: Distributions of signal amplitude, expresssed in ADC channels, in central points (A-E) of the sector *J1* (Quartz Fibres, foil, Hamamatsu PMT), exposed to 80 GeV electrons.

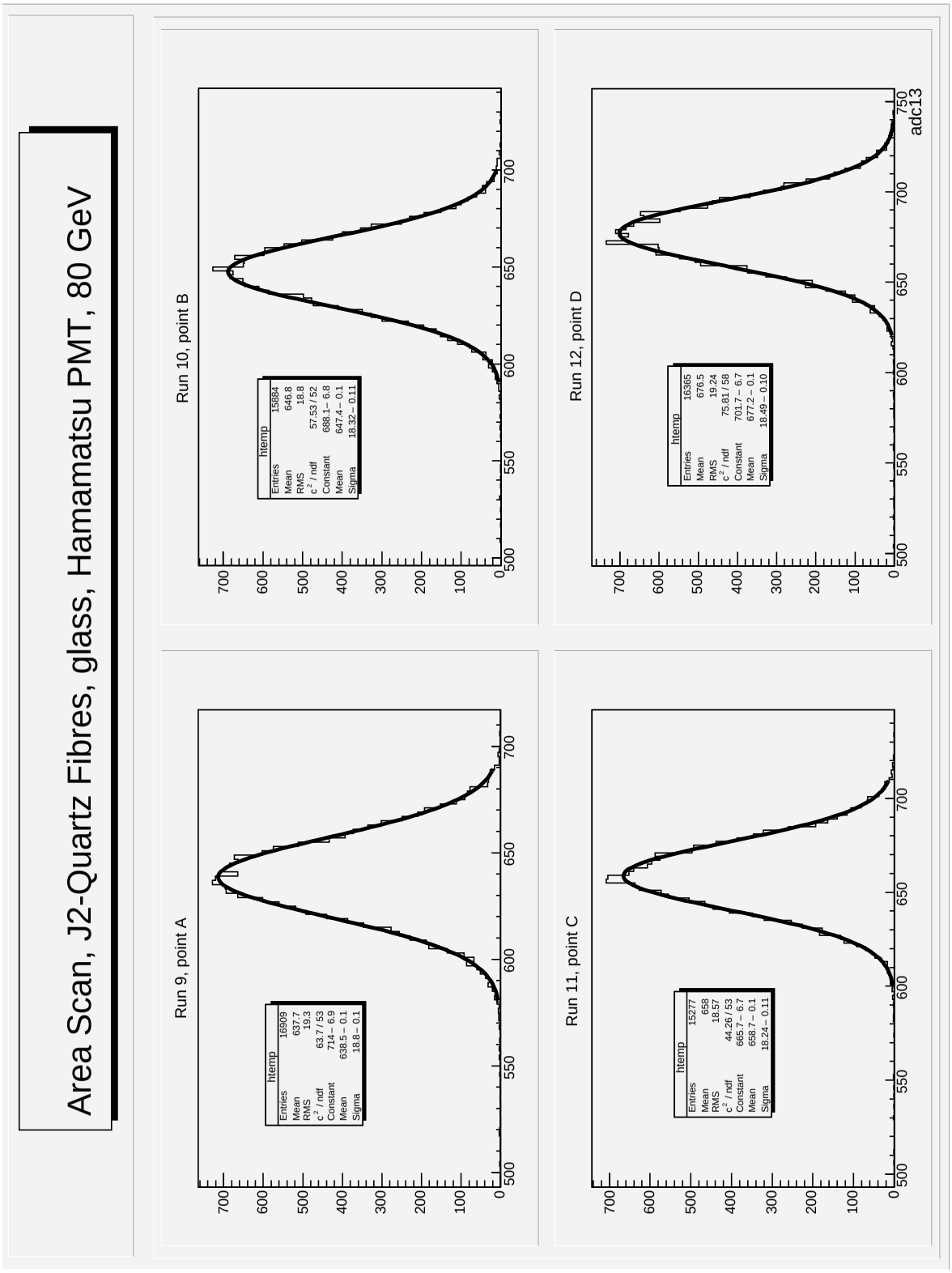

Figure 24: Distributions of signal amplitudes, expressed in ADC channels, in central points (A-E) of the sector *J2* (Quartz Fibres, glass, Hamamatsu PMT), exposed to 80 GeV electrons.

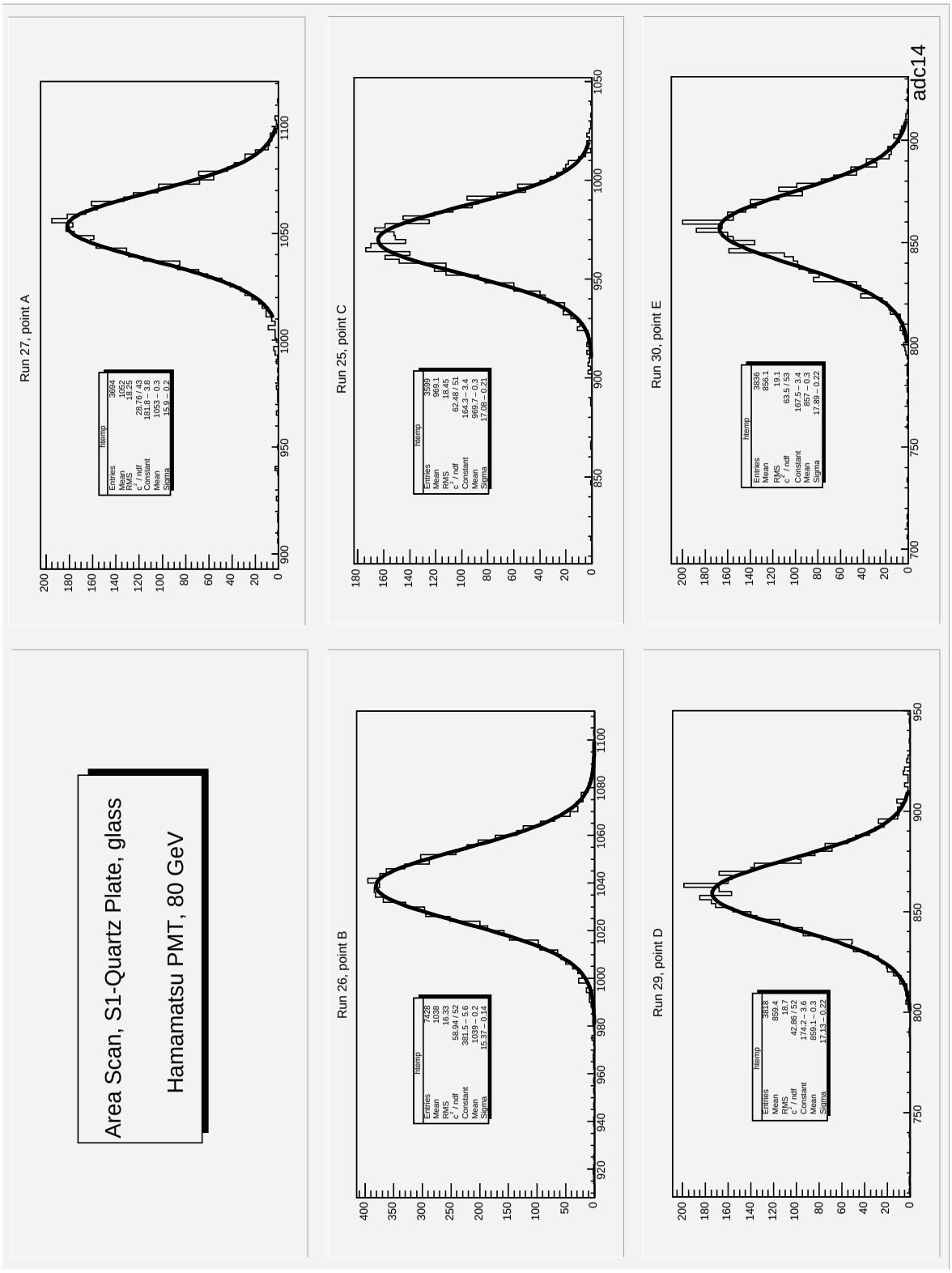

Figure 25: Distributions of signal amplitude, expressed in ADC channels, in central points (A-E) of the sector *S1* (Quartz Plate, glass, Hamamatsu PMT), exposed to 80 GeV electrons.

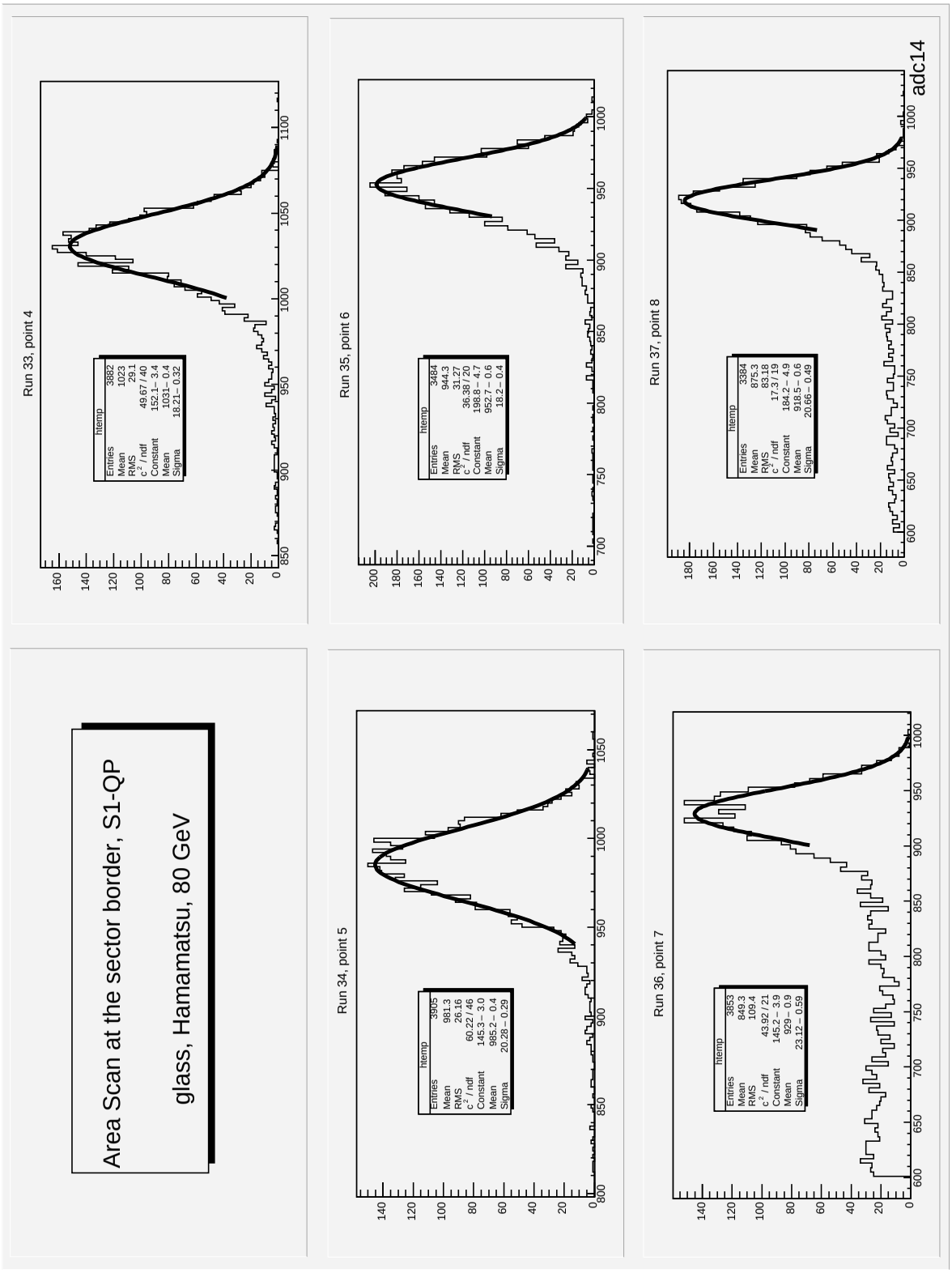

Figure 26: Distributions of signal amplitude, expressed in ADC channels, in border points (4-8) of the sector *S1* (Quartz Plate, glass, Hamamatsu PMT), exposed to 80 GeV electrons.

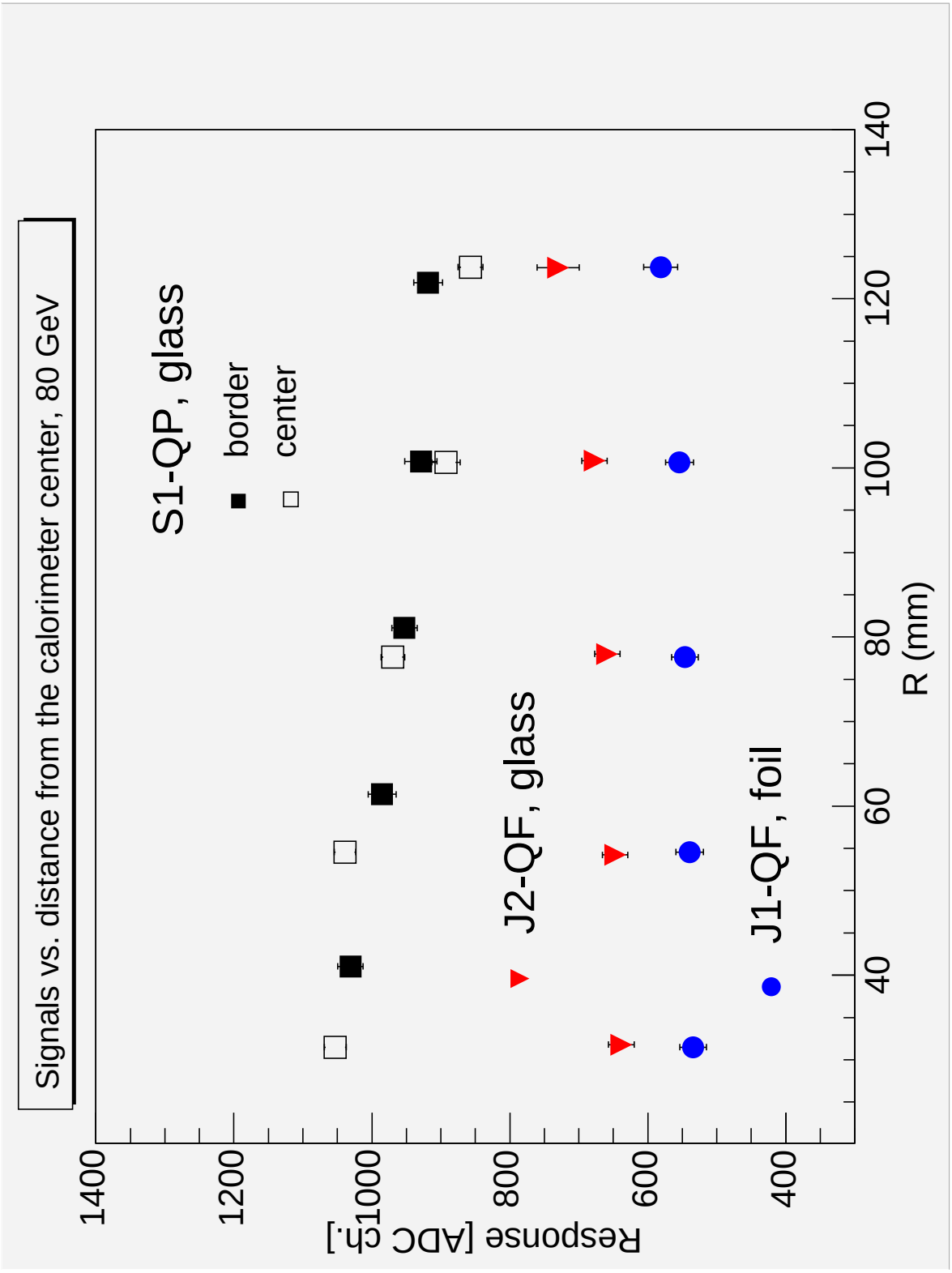

Figure 27: Comparison of calorimeter response produced by 80 GeV electrons in several points (A-E) of *J2* (QF, glass), *J1* (QF-foil) and *S1* (QP-glass) sectors, all connected to Hamamatsu PMT. Dependence of calorimeter response on the distance from the calorimeter centre is shown.

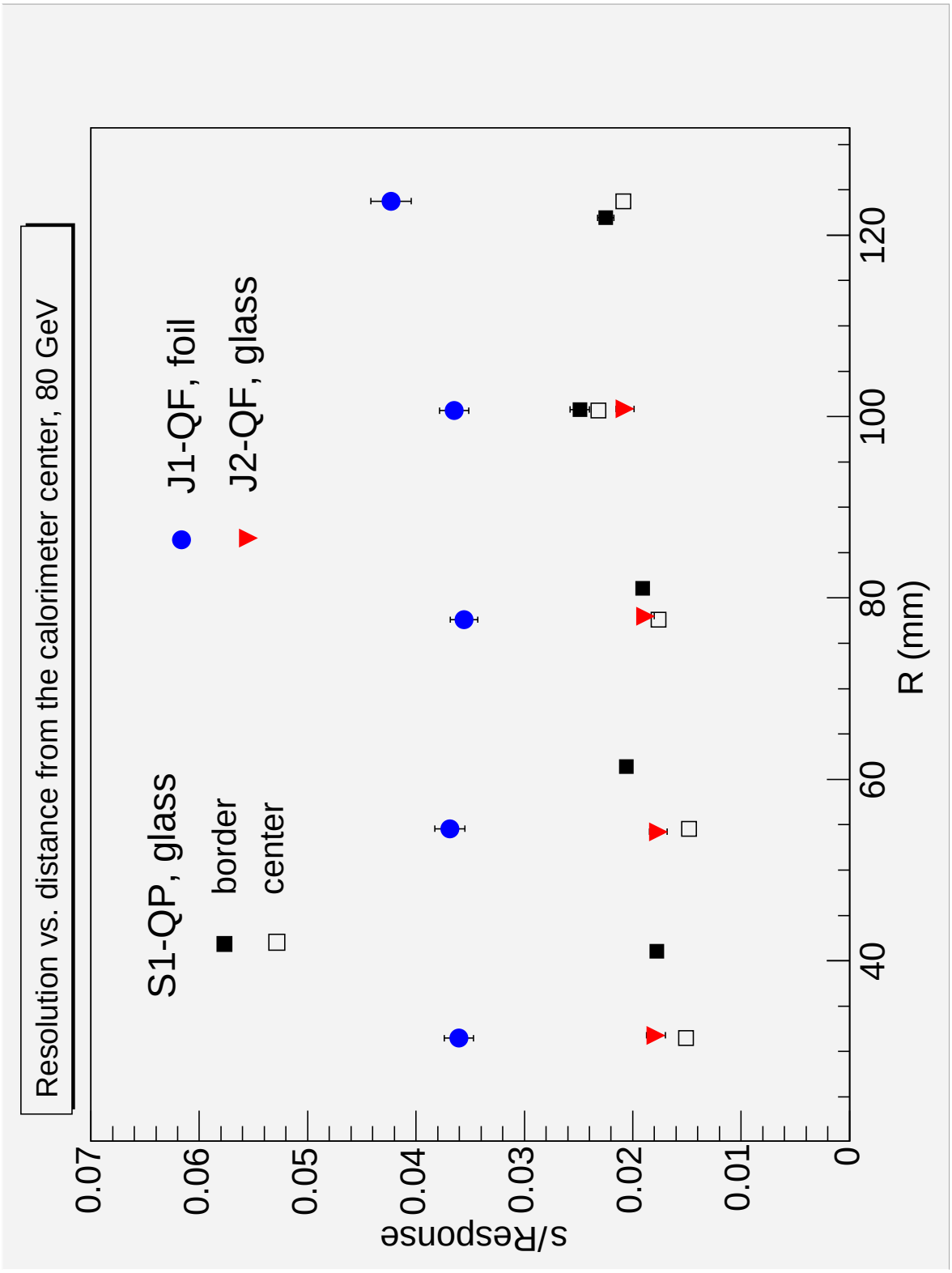

Figure 28: Comparison of calorimeter resolution to 80 GeV electrons in several points (A-E) of *J2* (QF, glass), *J1* (QF-foil) and *S1* (QP-glass) sectors, all connected to Hamamatsu PMT. Dependence of calorimeter resolution on distance from the calorimeter centre is shown.

Table 1: Linearity and energy resolution of the CASTOR calorimeter prototype. Parameters for two fits are shown: (1) $\sigma/E = p_0 + p_1/\sqrt{E}$; (2) $\sigma/E = p_0 \oplus p_1/\sqrt{E} \oplus p_2/\sqrt{E}$.

	RESOLUTION					LINEARITY		
	fit	p_0	p_1	p_2 [GeV]	χ^2/ndf	a	b	χ^2/nd
Quartz Plate								
S1, glass	1	0.00 ± 0.02	0.36 ± 0.02		6.4/4	37.0 ± 12.1	7.7 ± 0.8	4.2/4
Philips PMT	2	0.01 ± 0.04	0.38 ± 0.04	0.42 ± 0.20	7.4/3			
Advanced Photonic	1	0.01 ± 0.05	0.28 ± 0.04		2.5/3	32.5 ± 2.4	4.3 ± 0.5	2.2/3
APD	2	0.03 ± 0.06	0.20 ± 0.04	1.25 ± 0.20	6.2/2			
Quartz Fibres								
S2, glass	1	0.00 ± 0.03	0.45 ± 0.04		3.2/4	3.6 ±	4.6 ±	0.41/4
Philips PMT	2	0.01 ± 0.06	0.48 ± 0.04	0.83 ± 0.20	3.7/3			
Quartz Fibres								
J2, glass	1	-0.00 ± 0.01	1.16 ± 0.13		4.1/4	9.3 ±	1.3 ± 0.6	6.5/4
Hamamatsu APD	2	0.04 ± 0.02	0.82 ± 0.22	4.5 ± 1.6	1.3/3			

References

[1] A. L. S. Angelis for the CASTOR group, 3rd CMS Workshop on Forward Physics, CERN, 29-30 May 2002.

[2] A. D. Panagiotou for the CASTOR team, CMS/TOTEM meeting on Diffraction, CERN, 6 December 2002.

[3] K. Eggert, Meeting on Physics at LHC, Prague 6-12, July 2003; Nucl. Phys. **B122** (2003) 447.

[4] E. Gładysz-Dziaduś for the CASTOR group, Nuclear Theory'21 by V. Nikolaev, Heron Press, Sofia, 2002, p.152-175; A.L.S. Angelis et al., J. Phys. **G28** (2002) 1937.

[5] A. D. Panagiotou, talk at CPT Week, PRS-HI meeting, November, 2003 and CMS Week-HF meeting, August, 2003, CERN.

[6] E. Gładysz-Dziaduś, Phys. Part. Nucl. **34** (2003) 285-347; Fizika Elementarnykh Chastis i Atomnogo Yadra **34** (2003) 565-678.

[7] S.A. Sadovsky et al., Phys. Atom. Nucl. **67** (2004) 396-405; Yad. Fizika **67** (2004) 414-424.

[8] E. Gładysz-Dziaduś, CMS-Heavy Ion Meeting International Workshop on Physics and Techniques for the LHC and RHIC Experiments, *dedicated to A. Angelis*, Delphi, Greece, June 2003.

[9] M. Livan, V. Vercesi and R. Wigmans, CERN 95-02, 1995.

[10] G. Anvinzino et al., Meth. Phys. Res. **A357**(1999)350-362.

[11] G. Anvinzino et al., Meth. Phys. Res. **A357**(1995)369.